PB81-196594

Development of Measurement Methodology for Evaluating Fugitive Particulate Emissions

SRI International
Menlo Park, CA

Prepared for

Environmental Sciences Research Lab.
Research Triangle Park, NC

May 81

U.S. Department of Commerce
National Technical Information Service
NTIS

TECHNICAL REPORT DATA
(Please read Instructions on the reverse before completing)

1. REPORT NO. EPA-600/2-81-070	2.
3. RECIPIENT'S ACCESSION NO. PB81 196594	
4. TITLE AND SUBTITLE DEVELOPMENT OF MEASUREMENT METHODOLOGY FOR EVALUATING FUGITIVE PARTICULATE EMISSIONS	5. REPORT DATE May 1981
	6. PERFORMING ORGANIZATION CODE
7. AUTHOR(S) E.E. Uthe, J.M. Livingston, C.L. Witham, N.B. Nielsen	8. PERFORMING ORGANIZATION REPORT NO.
9. PERFORMING ORGANIZATION NAME AND ADDRESS SRI International 333 Ravenswood Avenue Menlo Park, California 94025	10. PROGRAM ELEMENT NO. C07A1D/07-0372 (FY-80)
	11. CONTRACT/GRANT NO. Contract 68-02-2752
12. SPONSORING AGENCY NAME AND ADDRESS Environmental Sciences Research Laboratory - RTP, NC Office of Research and Development U.S. Environmental Protection Agency Research Triangle Park, North Carolina 27711	13. TYPE OF REPORT AND PERIOD COVERED
	14. SPONSORING AGENCY CODE EPA/600/09
15. SUPPLEMENTARY NOTES	

16. ABSTRACT

A measurement methodology to evaluate fugitive particulate emissions was developed and demonstrated. The project focused on the application of the lidar (laser radar) technique under field conditions, but in circumstances that simplified and controlled the variables of the general problem.

The lidar was used to make elevation scans perpendicular to an aerosol plume generated by controlled release of particulate material into the atmosphere. The lidar backscatter and these values were related to independently measured particulate emission rates. Very high correlation was obtained between time-averaged lidar observations and emission rates (correlation coefficients of 0.9 or better in most runs), with substantially less correlation for individual lidar observations. Relatively high correlation also was obtained between smoke reader data (opacity) with smoke emission rate and with lidar backscatter. For dense smokes, attenuation of the lidar energy was shown to be of importance in interpreting data in terms of smoke concentration.

The lidar was used at the site of an actual fugitive particulate source to demonstrate that appropriate data can be collected for measurement of source emission rate.

17. KEY WORDS AND DOCUMENT ANALYSIS

a. DESCRIPTORS	b. IDENTIFIERS/OPEN ENDED TERMS	c. COSATI Field/Group

18. DISTRIBUTION STATEMENT RELEASE TO PUBLIC	19. SECURITY CLASS *(This Report)* UNCLASSIFIED	21. NO. OF PAGES
	20. SECURITY CLASS *(This page)* UNCLASSIFIED	22. PRICE

EPA Form 2220-1 (Rev. 4-77) PREVIOUS EDITION IS OBSOLETE

PB81-196594

EPA-600/2-81-070
May 1981

DEVELOPMENT OF MEASUREMENT METHODOLOGY FOR EVALUATING FUGITIVE PARTICULATE EMISSIONS

by

Edward E. Uthe
John M. Livingston
Clyde L. Witham
Norman B. Nielsen

SRI International
Menlo Park, California 94025

Contract 68-02-2752

Project Officer

William D. Conner
Emission Measurement and Characterization Division
Environmental Sciences Research Laboratory
Research Triangle Park, North Carolina 27711

ENVIRONMENTAL SCIENCES RESEARCH LABORATORY
OFFICE OF RESEARCH AND DEVELOPMENT
U.S. ENVIRONMENTAL PROTECTION AGENCY
RESEARCH TRIANGLE PARK, NORTH CAROLINA 27711

PRODUCT OF:
NATIONAL TECHNICAL
INFORMATION SERVICE
U.S. DEPARTMENT OF COMMERCE
SPRINGFIELD, VA. 22161

DISCLAIMER

This report has been reviewed by the Environmental Sciences Research Laboratory, U.S. Environmental Protection Agency, and approved for publication. Approval does not signify that the contents necessarily reflect the views and policies of the U.S. Environmental Protection Agency, nor does mention of trade names or commercial products constitute endorsement or recommendation for use.

ABSTRACT

A measurement methodology to evaluate fugitive particulate emissions was developed and demonstrated. The project focused on the application of the lidar (laser radar) technique under field conditions, but in circumstances that simplified and controlled the variables of the general problem.

The lidar was used to make elevation scans perpendicular to an aerosol plume generated by controlled release of particulate material into the atmosphere. The lidar backscatter signatures were processed in terms of cross-plume integrated-backscatter and these values were related to independently measured particulate emission rates. Very high correlation was obtained between time-averaged lidar observations and emission rates (correlation coefficients of 0.9 or better in most runs), with substantially less correlation for individual lidar observations. Relatively high correlation also was obtained between smoke reader data (opacity) with smoke emission rate and with lidar backscatter. For dense smokes, attenuation of the lidar energy was shown to be of importance in interpreting data in terms of smoke concentration.

Finally, the lidar was used at the site of an actual fugitive particulate source to demonstrate that appropriate data can be collected for measurement of source emission rate.

This report was submitted in fulfillment of Contract 68-02-2752 by SRI International under sponsorship of the U.S. Environmental Protection Agency. This report covers the period 30 September 1977 to 15 January 1981 and work was completed as of 15 January 1981.

CONTENTS

Abstract iii
Figures vi
Tables viii
Acknowledgments ix

1. Introduction 1
2. Summary and Conclusions 3
3. Recommendations 5
4. Plume Experiment and Analysis Method 7
    General 7
    Mark IX lidar system 7
    Aerosol generation 9
    Field application 27
    Analysis method 28
5. Results 31
    Camp Park results 31
    Woodland results 33
6. Observations at a Fugitive Emissions Source 53

References 56
Appendix

Data tabulation 57

Preceding page blank

FIGURES

Number		Page
1	SRI International's Mark IX mobile lidar system	8
2	Example of computer-generated profiles of vertical plume density	8
3	Feeder calibration for Min-U-Sil	12
4	Aerosol dispersion system	14
5	Dust disperser	15
6	Controlled silica dust plumes generated to represent fugitive emission sources	16
7	CARB smoke generator with SRI stack modification	18
8	Calibration of CARB transmissomer in terms of aerosol mass concentration for white smoke	20
9	Calibration of CARB transmissometer in terms of aerosol mass concentration for black smoke	20
10	White smoke generation from smoke pots and candles.	22
11	Method of evaluating aerosol mass concentration of emissions from smoke pots and candles	23
12	Particle size distribution as measured in the laboratory	25
13	Mark IX laser laser calibration, Woodland, California, 15 August 1979	29
14	Particulate emission rate evaluated from lidar, plotted as a function of emission rate as evaluated from the particle feeder	32
15	Lidar, emission, and smoke reader data for CARB black smoke (9 August 1979, 1805-1838 PDT)	36

Number		Page
16	Lidar, emission, and smoke reader data for CARB black smoke (9 August 1979, 1838-1910 PDT)	38
17	Lidar, emission and smoke reader data for CARB black smoke (combined runs)	40
18	Lidar, emission, and smoke reader data for smoke pots (10 August 1979, 1646-1731 PDT)	41
19	Lidar, emission, and smoke reader data for smoke pots (10 August 1979, 1738-1818 PDT)	42
20	Lidar, emission, and smoke reader data for smoke pots (10 August 1979, 1827-1902 PDT)	43
21	Lidar, emission, and smoke reader data for smoke pots (combined runs)	45
22	Lidar, emission, and smoke reader data for smoke candles (15 August 1979, 1923-1949 PDT)	46
23	Lidar, emission, and smoke reader data for smoke candles (16 August 1979, 1935-2008 PDT)	48
24	Lidar, emission, and smoke reader data for smoke candles (combined runs)	49
25	Lidar opacity analysis for smoke pot plumes	51
26	Lidar location and viewing direction during cement plant observations, 21 May 1980	54
27	Vertical plume cross sections made about 500 m downwind of the Permanente Cement plant on 21 May 1980	55

TABLES

Number		Page
1	Particle Size Properties of Min-U-Sil	10
2	Pressure Drop for Various Types of Tubing While Conveying 5-μm Min-U-Sil	13
3	Aerosol Characteristics	26
4	Lidar Data Log--Smoke Observations	34
5	Linear Correlation Coefficients Squared (R^2)	50

ACKNOWLEDGMENTS

This study was funded by the U.S. Environmental Protection Agency, with William D. Conner of the Emissions Measurement and Characterization Division (Environmental Sciences Research Laboratory) as Project Monitor. We thank Mr. Conner for his valuable advice in conducting the study. Special thanks are due the State of California--especially Mr. Robert Varner--for making available their smoke generator and for providing trained smoke reader observations.

SECTION 1

INTRODUCTION

The total source strength of pollution emitted by industrial plants is the aggregate of all diffuse and minor specific emissions, as well as major identifiable point sources. Therefore, for many plants, measurement of individual emissions from the multiplicity of sources is neither economical nor practical.

The only feasible approach is to measure, as accurately as possible, the concentration throughout a cross section of the downwind "plume" of the combined fugitive emissions, to integrate these, and, from a measurement of the integrated wind velocity through the plane of the cross section, to calculate the pollutant mass flow.

The problems of accomplishing such measurements with existing technology are many. Specifically, with in-situ samplers it is virtually impossible to characterize adequately the concentration of particles throughout the total cross section of the plume, or to relate any measurements made to the total envelope of the plume, or to determine its extent. This is especially the case above the surface, because of the extended and variable nature of the multiple sources of fugitive emissions. For particulate fugitive emissions, any deposition or transformation in the intervening distance must also be considered in order to derive an estimate of the total source strength.

Lidar (laser radar) observation fulfills, as no other method does, the requirement for delineating the spatial distribution of elevated particulate pollution plumes and for readily distinguishing between pollution background and pollution from the source being studied. While there are limitations and difficulties in using lidar backscatter measurements for determining absolute particulate concentrations, it is possible to evaluate, with useful accuracy, the near-instantaneous distribution of particulate material within a selected cross section or envelope. It is thus possible to derive a series of such cross sections in time and, from a measurement of mean wind velocity and information on the backscatter-to-concentration ratio, to derive an estimate of source emission rate.

The objective of this study, conducted by SRI International (SRI) under contract to the U.S. Environmental Protection Agency (EPA), was to develop and demonstrate a measurement methodology with which to evaluate fugitive particulate emissions. The method was to be capable of measuring the flow of total particulate pollution downwind of an industrial plant by using both

surface sampling and remote sensing techniques for sampling above the surface level. Specifically, the program focused on the application of the lidar technique under field conditions, but in circumstances that simplified and controlled the variables of the general problem. A demonstration program was conducted to show the general applicability, accuracy, and limitations of the lidar technique for measuring fugitive emissions. This report presents the method of approach, describes the experimental studies, and discusses the results obtained.

SECTION 2

SUMMARY AND CONCLUSIONS

SRI, under contract to EPA, conducted three experimental field programs designed to demonstrate a lidar methodology for measurement of fugitive particulate emissions. The first field program used controlled releases of silica powder to simulate particulate emissions from a fugitive sources. A lidar system (SRI Mark IX) was used to make elevation scans perpendicular to the transport direction of the aerosol plume about 500 m downwind of the source. The lidar backscatter signatures for each elevation scan were processed for values of cross-plume integrated-backscatter, and these values were related to independently measured particulate emission rates. Results showed that integrated backscatter generally increases linearly with particulate emission rate; however, relatively large scatter of the data between these quantities occurred, probably caused by emission rate variations. These results formed the basis of a more extensive experimental program designed to extend the applicability of the technique.

A second field program was conducted using black and white smoke from a combustion generator (operated for the training of smoke inspectors) and smoke pots and candles. The smoke emission rate for the pots and candles was determined by the number of units ignited. In addition to the lidar observations, a trained smoke inspector was used to estimate plume opacity downwind of the source.

Only limited data were collected with the combustion generator because of its low emission rates and because the white smoke mostly was evaporated at the downwind distance of the lidar observations. Very high correlation was obtained between time-averaged lidar observations and black-smoke emission rate (squared-correlation coefficients R^2 greater than 0.95), with substantially less correlation obtained between individual lidar observations and smoke emission rate. Smoke reader data (taken near the stack) were also highly correlated with the smoke emission rate.

A series of experiments was also conducted using commercially available smoke pots and candles. The quantity of smoke was varied by igniting 1, 2, 4, or 8 units. For these experiments, the trained smoke reader made opacity observations downwind of the source, at approximately the location from which the lidar viewed the plume. For three experimental runs with smoke pots, R^2 correlation values of 0.91, 0.78, and 0.75 were obtained between time-averaged lidar data and emission rate, while values of 0.95, 0.88, and 0.37 were obtained between smoke reader data and emission rate. However, because of the high density of the smoke produced by the smoke pots, significant

attenuation of the laser energy was evident. A factor of two increase in emission rate resulted in substantially less than a factor of two increase in cross-plume integrated lidar backscatter. Experiments with lower density smoke from smoke candles provided expected one-to-one correspondance between lidar response and smoke emission rate.

Plume opacities derived from the lidar data by analysis of the clear-air returns on the far side of the plume returns were substantially less than those estimated by the smoke reader. Correction applied because of the longer wavelength lidar and submicron smoke particles explained only a part of the difference between lidar and smoke reader observations.

A third field program was conducted to demonstrate use of the lidar system at an actual fugitive emissions source. The lidar was used successfully to make downwind vertical-scans across the particulate plume generated by the Permanente Cement Plant located in Cupertino, California. The data were collected in the same manner as for the test smokes and therefore, can be processed in the same manner as the test data to estimate plant particulate emission rates.

In summary, the major conclusions of this study are:

- Cross-plume integrated backscatter evaluated from data collected by scanning a lidar system across a downwind smoke plume behaved in a predictable manner with variations in particulate emission rate.
- Correlation between downwind lidar observations and source emission rate was greatly increased by averaging data from multiple lidar observations--typically 3 to 4 lidar elevation scans over a 5- to 10-minute period
- For low density plumes, the lidar responded linearly in a one-to-one manner with changes of particulate emission rate. Linear correlation coefficients greater than 0.9 were obtained in most cases.
- For higher density plumes, the lidar signal increased with increasing particulate emission rate but at less than one-to-one because of extinction processes.
- Correlation between downwind lidar observations and particulate emission rate was only slightly improved when corrections for wind speed variations (measured at the lidar site) were applied.
- Testing of lidar methodology was best accomplished using commercially available smoke candles. The quantity of smoke was controlled by the number of units ignited.
- Downwind plume opacities evaluated by a trained Method 9 observer were highly correlated with particulate emission rate and with the lidar cross-plume integrated backscatter.
- A mobile lidar system can successfully make appropriate cross-plume observations at actual fugitive particulate emission sources.

SECTION 3

RECOMMENDATIONS

This study demonstrated a methodology, using the lidar technique, for measurement of fugitive particulate emissions. Several additional studies suggested to further develop and demonstrate the lidar technique for this purpose are discussed below:

- In-Situ Measurement of Backscatter-to-Mass Concentration Ratio--This study showed that the cross-plume integrated backscatter evaluated by scanning a lidar system across an aerosol plume responds in a predictable manner with particulate emission rate. However, measurement of the absolute emission rate requires calibration of the lidar backscatter in terms of aerosol concentration. An in-situ measurement of the backscatter-to-mass concentration ratio would provide the needed calibration. In addition, the measurement of the variability of this ratio for different types of particles would provide an estimate of the accuracy of lidar measurement for the case of particle characteristics changing in the vertical. Therefore, we recommend that an instrument that measures absolute values of backscatter-to-mass concentration be developed.
- Airborne Lidar Measurement of Particulate Emissions from Large-Area Sources--Many fugitive emission sources, including coal mining, oil refiner, and cement plant operations, generate a particulate plume with large horizontal and vertical extent. For these sources, the pollution plume is more readily observed with an airborne lidar than with a surface-based system. A downward-pointing lidar could be flown along a path that encompasses the plant site to observe upwind and downwind particulate flow. Observations made in complex terrain sites would be greatly simplified as compared with those using a surface-based lidar. A two-wavelength airborne lidar system has recently been demonstrated (Uthe et al., 1980). Backscatter data at two wavelengths may provide the necessary information to estimate absolute mass concentration of observed aerosols. We recommend that an airborne lidar system be considered for measurement of particulate fugitive emissions.
- Choice of Lidar Wavelength or Wavelengths--Successful use of the lidar technique for remote measurement of particulate concentration requires knowledge of the relation between aerosol optical and physical parameters. Because fugitive emissions frequently comprise emissions from several source types, and the percentage of particulate from each type may vary, the particle characteristics (size, shape,

and composition) may also vary in both space and time. The backscatter-to-concentration ratio is dependent on these particle characteristics and, therefore, a fugitive emissions lidar system must be designed to be insensitive to changes of particle characteristics. We recommend that experiments be conducted to establish the proper wavelength or wavelengths for minimizing the effect of particle characteristics on the backscatter-to-concentration ratio.

SECTION 4

PLUME EXPERIMENT AND ANALYSIS METHOD

GENERAL

A program was planned to develop a measurement methodology for evaluating fugitive particulate emissions that used the unique capabilities of the lidar technique. A series of field experiments were designed to demonstrate the methodology by making measurements of an aerosol plume generated by continuous release of particulate material of known properties into the atmosphere at known rates. Therefore, the methodology was demonstrated under actual field conditions but simplified to the extent that the source of the particulate plume observed could be controlled at known emission rates. The primary purpose of this study was to demonstrate that lidar-observed quantities can be related in a predictable manner to the source emission rate.

MARK IX LIDAR SYSTEM

Lidar (Light Detection and Ranging) uses laser energy in radar fashion to observe remote atmospheric constituents effectively. The lidar system used to develop methodologies for fugitive dust measurement was SRI International's Mark IX mobile system, designed for use with atmospheric research programs. Figure 1 presents views of the lidar system, a block diagram, and a list of specifications. The lidar is installed within an 18-foot transport van complete with real-time data processing and display capabilities as well as with power-generating equipment, enabling operation at any site.

Figure 2 is an example of an intensity-modulated video display depicting the cross-plume aerosol structure observed by scanning the lidar in elevation. The brightness of this display is proportional to the logarithm of the backscattered light detected by the lidar system. Clearly, lidar can be used to map relative aerosol density distributions over remote distances. Computer-generated vertical-concentration profiles are plotted on the cross section for locations indicated by the cursor marks drawn above the plume return. Similarly, the backscattered data can be spatially integrated to determine a relative cross-plume density. Light that is elastically backscattered from suspended atmospheric particulate matter, as a function of pulse-transmission time, is quantitatively related to (clear air and plume) optical parameters along the observed path according to the lidar (radar) equation:

$$P(R) = KE\beta(R)^{-2}T^2(R) \quad , \qquad (1)$$

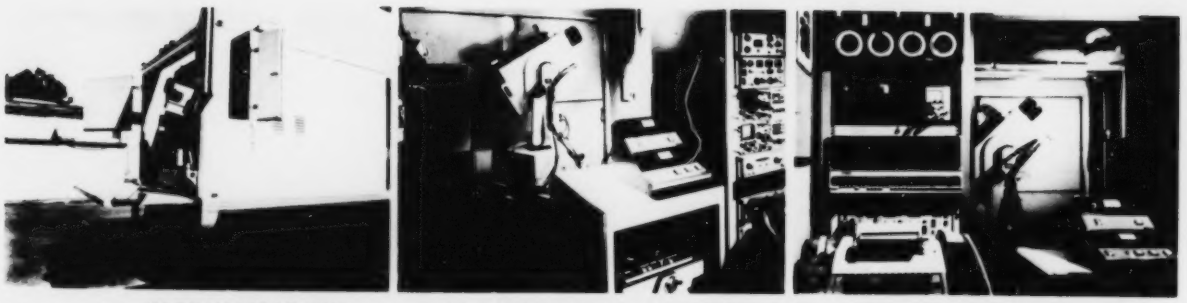

(a) MARK IX LIDAR VAN (b) ANALOG DATA AND FIRE CONTROL ELECTRONICS (c) DIGITAL DATA ELECTRONICS AND TV DISPLAY

EXTERIOR AND INTERIOR VIEWS OF THE LIDAR VAN

BLOCK DIAGRAM OF THE LIDAR SYSTEM

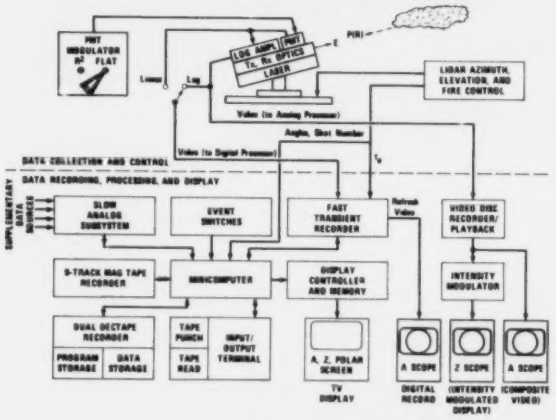

LIDAR SPECIFICATIONS

TRANSMITTER

6943Å Wavelength
0.5 mrad Beamwidth
1.0 J Pulse Energy
30 ns Pulse Length
60 ppm Maximum PRF

RECEIVER

6 inch Newtonian
1 to 5 mrad Field of View
5Å Predetection Filter
RCA 7265 PMT Detector
4-decade, 35-MHz Logarithmic Amplifier, Inverse-range-squared or step-function PMT modulation.

DATA SYSTEMS

Analog video disc recording (4.5 MHz) with A-scope and Z-scope real-time displays. Digital magnetic tape (data and programs) recording (25 MHz) with computer processing and real-time TV display (512 x 256 x 4 bit) of processed data.

MOUNT

Automatic azimuth and elevation fire and scan with 0.1° minimum resolution. Automatic reset. Mechanical safety stops.

Figure 1. SRI International's Mark IX mobile lidar system.

Figure 2. Example of computer-generated profiles of vertical plume density.

Lidar is located at lower left corner. The height and distance scale is 75 m/div. Vertical concentrations of the plume (relative to clear air, with a scale of 10 dB/div) are plotted at the lower left and the horizontal position associated with each profile is plotted in the upper right.

where

P = received power from a scattering volume defined by the laser pulse

L = lidar calibration constant

E = transmitted power

β = backscatter coefficient of the scattering volume

R = range from lidar of the scattering volume

T = transmission to the scattering volume.

For relatively clear air, the attenuation term can normally be ignored ($T^2 = 1$), and P provides information on the distribution of particulate material in the atmosphere, as shown in Figure 2. However, the evaluation of physical density terms (such as mass concentration) requires relating the optical parameter β to the density. Unfortunately, backscatter-to-concentration ratios are dependent on the distributions of particle size, composition, and shape. Before these factors and the ways in which they can limit the accuracy of quantitative evaluations of plume density can be considered, the lidar observations must be shown to respond in a predictable manner to increases of plume density for a given aerosol type. On this project the Mark IX lidar was used to make cross-plume observations (in the manner shown in Figure 2) of controlled emission sources with known particulate properties. Methods used to generate the particulate plume are discussed below.

AEROSOL GENERATION

Three methods of aerosol generation were used on this study to derive particulate plumes consisting of finely divided silica, black and white smoke from the controlled combustion, and white smoke from smoke pots and candles. Aerosol generation and particulate properties are discussed below.

Silica Powder

An aerosol generator was constructed for releasing fine silica powder to the atmospher at 1-m, 3-m, and 10-m height levels. This aerosol was generated by metering the powder into an 85 l/min (3 ft^3/min) air stream with a grooved-disk feeder and conveying the particle-laden air stream to the desired release level. At the release level the air stream was further diluted with a sonic velocity compressed-air jet to achieve dispersion of the powder particles.

Powder

A commercially available silica powder Min-U-Sil® (a product of PGS Floridin, a subsidiary of ITT, 3 Penn Center, Pittsburgh, Pennsylvania) was used as the source of the aerosol particles. Four grades of this powder are available, but only one (5 μm) was used here. Particle size data available on the various grades are summarized in Table 1.

Air permeability measurements indicated in Table 1 were made at SRI with a modified Fisher Sub-Sieve Sizer. Corrections are made for slip flow past small particles. Measurements of powder density were made on the 5-μm grade

TABLE 1. PARTICLE SIZE PROPERTIES OF MIN-U-SIL

Property	Min-U-Sil Grade Designation*			
	5 μm	10 μm	15 μm	30 μm
Sauter diameter				
From surface area (μm)†	1.10	2.06	2.70	4.20
From air permeability‡				
Porosity at which measured	0.562	0.514	0.514	--
Fisher diameter as measured (μm)	1.28	1.99	2.62	--
Fisher diameter, corrected§ (μm)	0.88	1.43	2.09	--
Mass median diameter (μm)†	1.9	3.5	4.0	8.8

*Approximately 98 percent of the mass is claimed by the manufacturer (PGS Floridin) to be finer than the diameter specified by the grade designation.

†As reported by the manufacturer.

‡As measured by SRI.

§Corrected for slip flow.

silica with a helium pycnometer. The measured density 2.64 g/cc agrees well with the expected 2.65 g/cc.

Moisture content of the powder used in the field was determined to be less than 0.1 percent.

Powder Feeder

The powder was metered by use of a proprietary grooved-disk feeder developed by SRI International. This disk feeder contained a circular groove 1/2-inch wide, 1/4-inch deep, and 4-inch diameter.

The powder was pneumatically unloaded from the groove with a metered air stream of 85 l/min. The grooved disk was rotated under the pneumatic pickup by means of a 1800-rpm Bodine Type NSH 12RG shunt-wound gearhead motor with a 240:1 gear ratio. The motor was coupled to the disk through a 1:3 pulley using a 3/8-inch wide notched belt. Feed rate was varied by the disk speed with a variable speed control (Minarik Model SL-15) connected to the drive motor.

The feeder system used in the field tests was designed to produce a wide range of feed rates without the necessity of changing groove size in the disk. Normal feed rates could be varied from approximately 4 kg/h to 25 kg/h.

During testing in the field, it was determined that a lower feed rate was desired. The feed rate was reduced to as low as 0.6 kg/h by placing a strip of 3/16-inch deep × 1/2-inch wide foam rubber into the groove to reduce its volume. Feed rates were nominally reduced by a factor of 3 (as determined by subsequent calibration in the laboratory) by reducing the groove volume while maintaining disk rotation speed.

Feeder calibrations were carried out to establish the feed rate as a function of disk speed on the 5-μm powder. The calibrations were conducted by collecting all the powder conveyed from the groove into a cloth bag filter. The collecting bag was weighed over timed intervals: These calibration data are shown in Figure 3. Feed rates are plotted as a function of disk rotation speed or drive motor shaft speed (which was conveniently measured in the field). From the calibration data, the porosity of the 5-μm powder in the feeder groove was calculated to range from 0.80 to 0.83.

Aerosol Dispersion

The 85 l/min dust-laden air stream from the feeder was introduced to a dispersion nozzle located at the desired atmospheric release level through either a 5/16-inch ID copper tube or 5/16-inch ID Tygon® tubing. Originally the copper tubing was used exclusively, but excessive plugging resulted, possibly because of a few kinks in this tubing. Other than during actual plugging of the tubing, mass flow rates were not affected by the type of tubing used.

To determine whether plugging was dependent on the type of tubing used to convey the silica to the disperser nozzle, pressure drops were measured with various types of tubing while conveying powder. Table 2 is a summary of those measurements. The reason for the difference in pressure drop for Tygon® and copper tubing when feeding dust was not investigated.

The conveying velocity within the 5/16-inch ID tube was 28.6 m/s. Since the longest length of tubing used was about 10 m, the residence time in the dispersion system was less than a second. Any fluctuation in feed rate caused by plugging in the conveying tube would then have a frequency of less than a second (unless the conveying tube plugged completely).

Dust-laden air from the feeder was conveyed to a disperser, where it was exposed to a 1130 l/min compressed air jet flowing from a 52 psig plenum pressure. Details of the aerosol dispersion system are shown in Figure 4. A vertical 1-inch aluminum tube was used to supply compressed air to the dispersion nozzle at the top. This tube was equipped with valves and unions so that the effective overall height of the system could be set at 1, 3, or 10 m. The dispersion system was supported by guy lines staked to the ground. Compressed air was supplied by a portable 100 ft^3/min compressor transported to the field test site.

Details of the dispersion nozzle are shown in Figure 5. No quantitative measurement of the degree of dispersion was made; however, previous studies with this type disperser showed good dispersion. Figure 6 is a photograph of the powder dispersion system emitting at the 1- and 10-m levels.

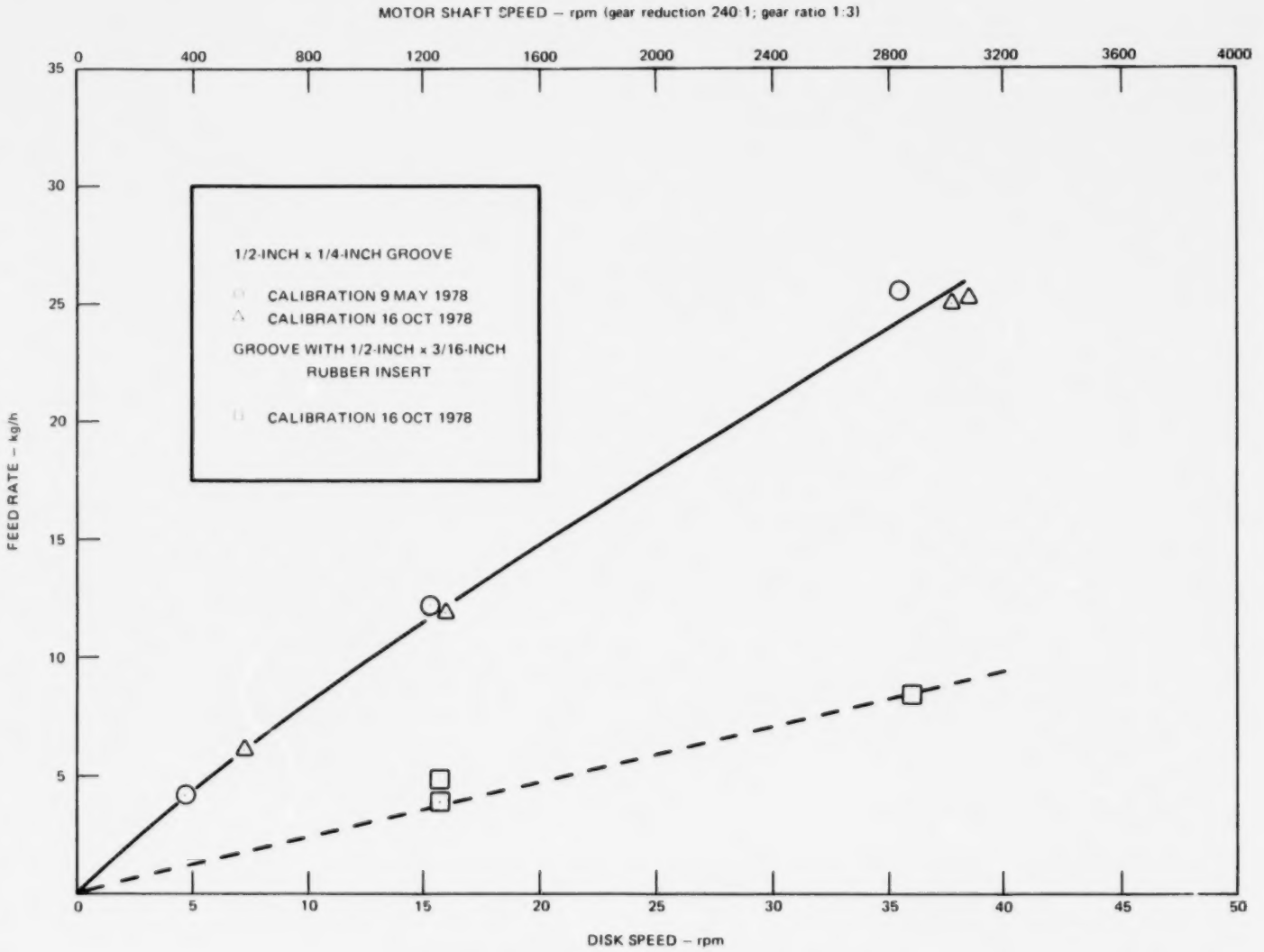

Figure 3. Feeder Calibration for 5-μm Min-U-Sil®

TABLE 2. PRESSURE DROP FOR VARIOUS TYPES OF TUBING WHILE CONVEYING 5-μm MIN-U-SIL*

Length of Tubing (ft)	Tubing ID (inches)	Tubing Type	Air Rate (ft^3/min)	Conveying Velocity (f/s)	Pressure Drop (psig)†	
					Not Feeding	Feeding
5	7/32	Polypropylene	3	192	2.2	6.5
			2	128	1.3	4.2
5	1/4	Tygon	3	147	2.1	6.8
			2	98	1.2	4.5
5	5/16	Tygon	3	94	1.2	5.0
			2	63	0.8	3.0
5	5/16	Copper	3	94	1.2	2.3
30	5/16	Tygon	3	94	3.5	11
			2	63	1.9	8.0
30	5/16	Copper	3	94	3.5	7.8

*Feed rate was approximately 25 kg/h.

†Pressure was measured in feeder compartment; hence includes the pressure drop across the dust pickup tube in the feeder.

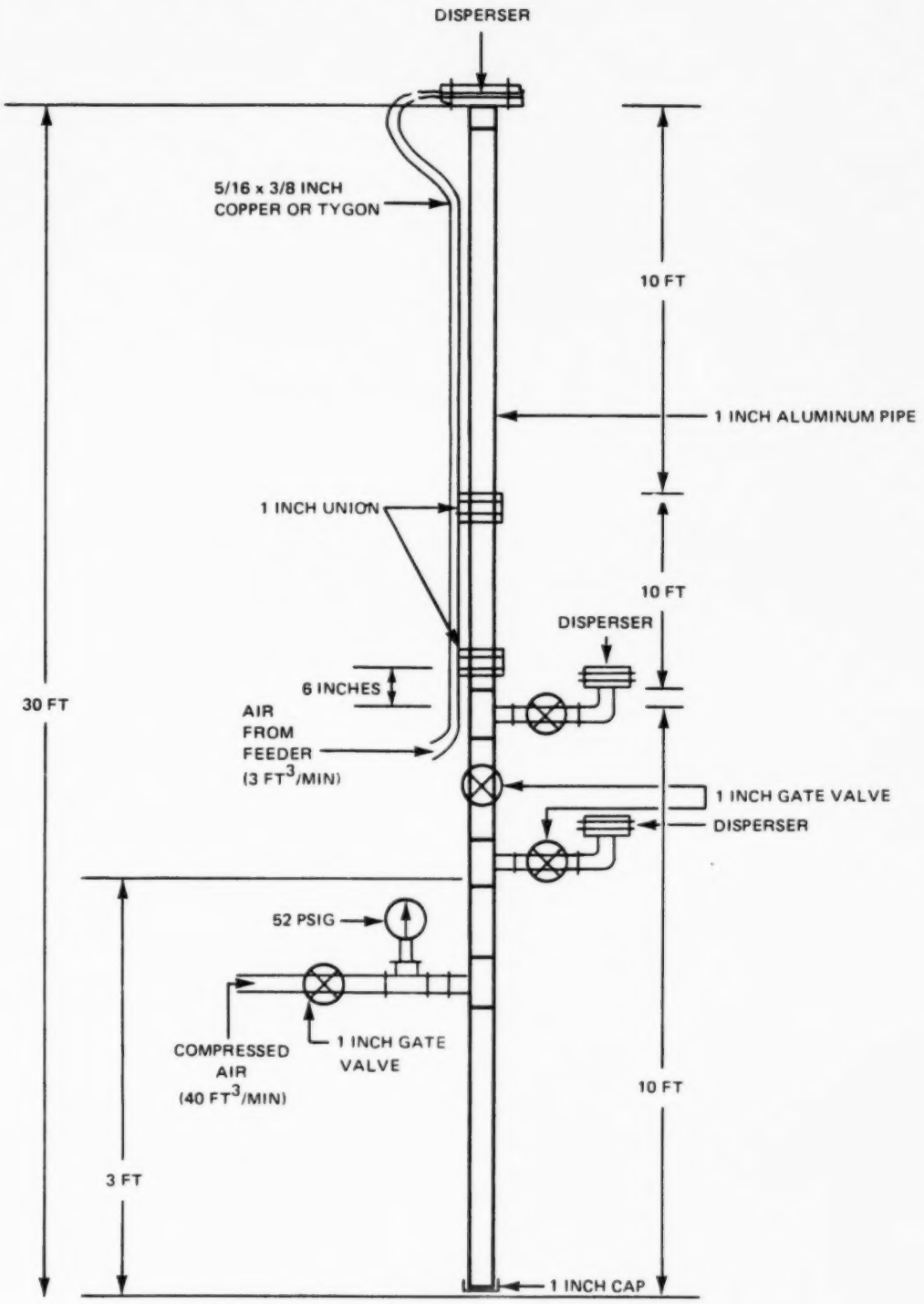

Figure 4. Aerosol dispersion system.

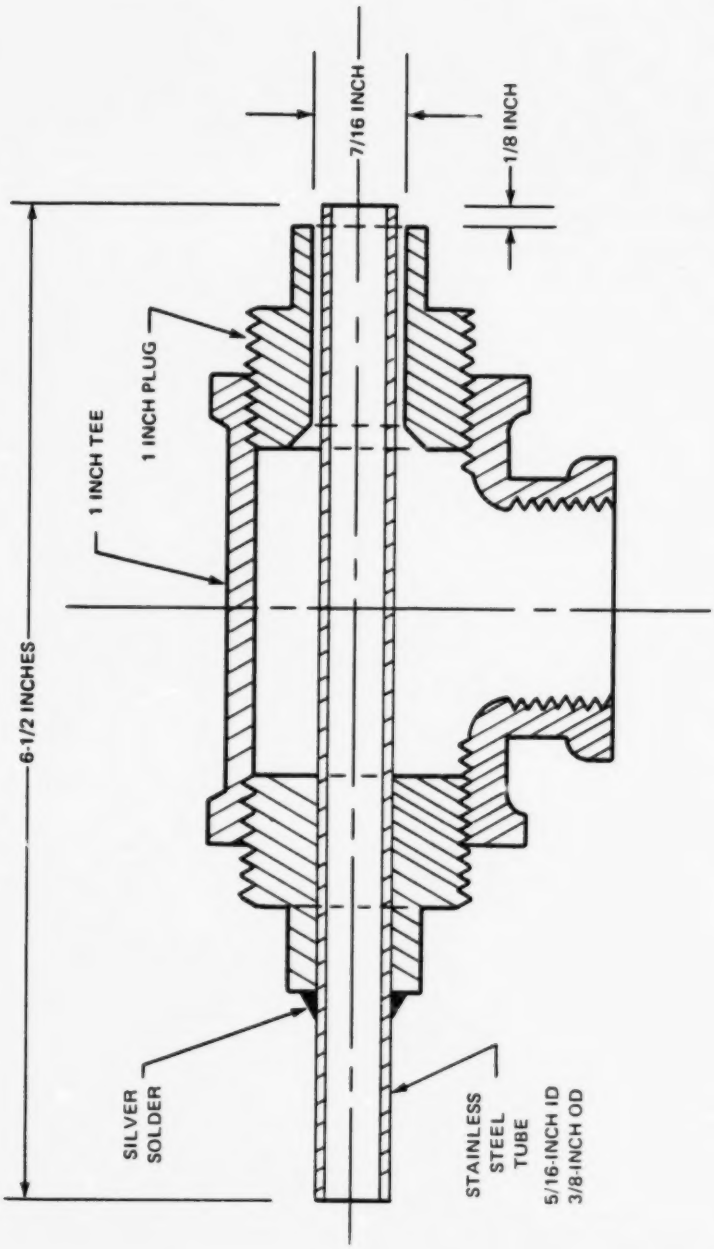

Figure 5. Dust disperser.

(a) EMISSION 1 m ABOVE SURFACE

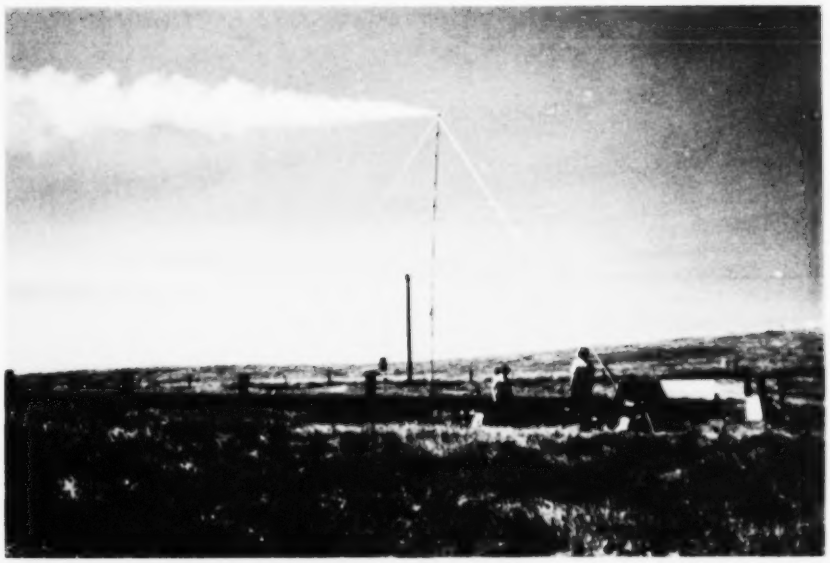

(b) EMISSION 10 m ABOVE SURFACE

Figure 6. Controlled silica dust plumes generated to represent fugitive emission sources.

Ambient Air Sampling

Nuclepore filter samples of the ambient air downwind of the discharge point were taken in a limited number of instances during field work. Samples were taken at distances ranging from approximately 15 to 100 meters downwind of the source. The low volume samples were taken at a flow rate of 2 l/min for approximately 10-min periods with portable battery-operated personal sampler pumps. Results were inconclusive because of the difficulty of maintaining the samplers in the proper location during variable winds for sufficiently long periods of time. Thus, additional field air sampling was discontinued. Samples taken generally indicated a ground-level particulate concentration at 100 m downwind of the emission point of 35 mg/m^3 per kg/h feed rate when fed at a 10-m height.

Black and White Smoke (CARB Generator)

A series of experiments were planned using a smoke generator owned by the State of California Air Resources Board (CARB). CARB uses the generator primarily for certifying smoke inspectors. Both a white smoke (produced by vaporization and condensation of diesel fuel) and a black smoke (produced by incomplete combustion of toluene) could be emitted from the smoke generator through a 17-ft high stack.

Because heights of 10 m and 1 m were specified for the lidar field test, modifications to the stack were required. In order to accommodate the two different emission levels, a 12-inch diameter, 28 gauge galvanized "tee", was attached to the top of the 17-ft stack. Two 8-ft sections of aluminum "flex" pipe were attached to the vertical branch of the tee and braced with a 2-inch aluminum angle to give an overall stack height of 34 ft. The 1-m emission level was accomplished by attaching 2 sections of 12-inch diameter aluminum flex pipe to the horizontal branch of the tee and then bending the pipe into the appropriate position. In order to divert the flow from one emission level to the other, a cap was placed over the end of the appropriate emission point.

Erecting and stabilizing the stack was a difficult process that required the help of several people and restricted use of the generator to one position in the field. Guy ropes were attached to the stack by 1-1/2-inch eyebolts, bolted to the stack at two levels. The stack configuration is shown in Figure 7.

White smoke is produced in the CARB smoke generator by injecting diesel fuel (No. 2 fuel oil) into the exhaust manifold of a 4-cycle, 3-horsepower gasoline engine run at full throttle. The diesel fuel is vaporized on contact with the hot exhaust gases of the gasoline engine and recondensed when mixed with dilution air from a blower.

Black smoke is produced by partial combustion of toluene inside a small metal cup. Toluene is continuously pumped to the cup. By restricting the amount of air available for combustion, carbon particles (soot) were produced and introduced to the stack through a blower.

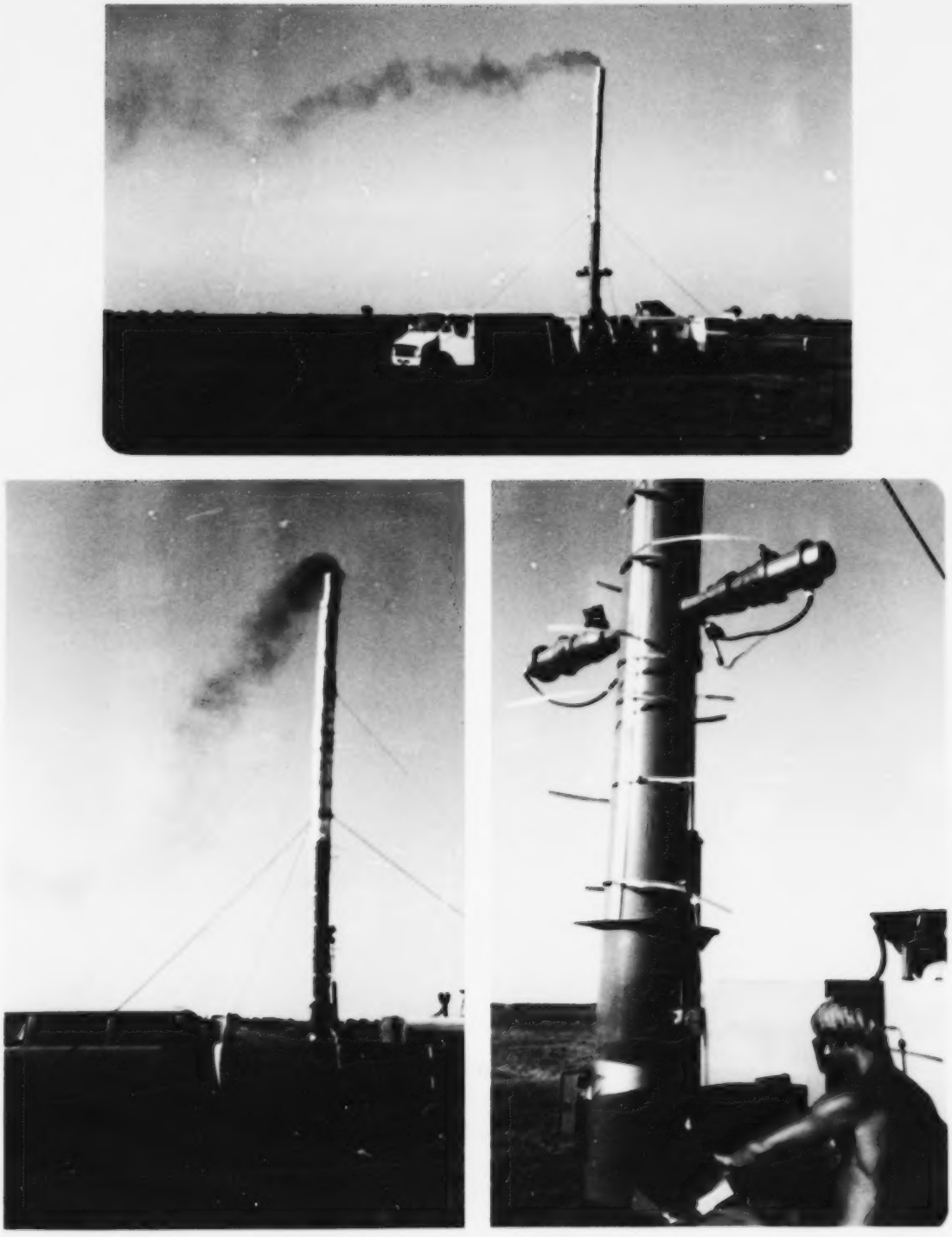

Figure 7. CARB Smoke Generator with SRI Stack Modification.

Total airflow through the stack was measured by placing a 10-inch diameter sharp-edged orifice, machined in 16 guage stainless steel, in the stack at a position where the stack folds for transport. Radius taps and a Magnehelic gauge were used to measure the pressure drop across the orifice. Total stack airflow was approximately 1000 ft^3/min. Liquid flowmeters were installed in the diesel and toluene feed systems to monitor mass flow into the system. The normal operating flows were 15-60 cc/min for diesel fuel and 50-175 cc/min for toluene.

The generator is equipped with a white light transmissometer with a path length of approximately 12 inches. The transmissometer was used to measure opacity in the stack and as a guide to set the liquid flow (diesel or toluene) for smoke production. The transmissometer is attached to the stack, and the optics are protected by clean airflows from two small blowers. The air from these blowers was not measured, but was assumed to be small compared to the main air flow.

Emission Rates

Aerosol mass emission rates for the CARB smoke generator were monitored with the transmissometer and determined by gramivetric analysis of samples collected on 25 mm, 0.4-μm pore-size Nuclepore filters. Filter measurements were taken at the outlet of the stack. The sampling airflow was provided by a vacuum pump and was controlled and measured using a calibrated critical flow orifice meter. The sampling rate was held constant at 2 l/min.

The Nuclepore filters allowed a sample time ranging from 0.5 to 5 minutes at a sampling rate of 2 l/min. This sample time was sufficient to deposit enough material on the filters so that the sample weight was approximately 30 percent of the filter tare weight. The white smoke plugged the filters much faster than the black smoke. All samples were taken on open face filters.

Figures 8 and 9 are plots of the experimental determinations of mass concentration for the white and black smokes as a function of the smoke generator transmissometer reading. These two figures are calibration curves for the two aerosol types, and were used to determine the mass emission rates for each CARB smoke generator test. The mass emission rate was determined from the mass concentration in the stack and the total airflow rate in the stack.

The white smoke from the CARB smoke generator was emitted at rates of 0.44 to 4.5 g/min in tests run with the lidar. The amount of aerosol actually produced was only about 8 to 15 percent of the total diesel fuel supplied to the generator. The remainder existed as a vapor in the air stream. Since the vapor pressure of the diesel is relatively high, the measured aerosol emission rates are only applicable at the outlet of the 10-m stack. As the cloud of aerosol moves downwind, the aerosol droplets will evaporate and eventually disappear. Since the droplets are submicron to begin with, the evaporation rate is high, and the aerosol cloud disappears quite rapidly. Visual estimates indicated that the cloud persisted only to about 100 m downwind. The ratio of diesel aerosol concentration at a given point downwind from the generator to the concentration as measured at the outlet of the stack is probably constant from run to run.

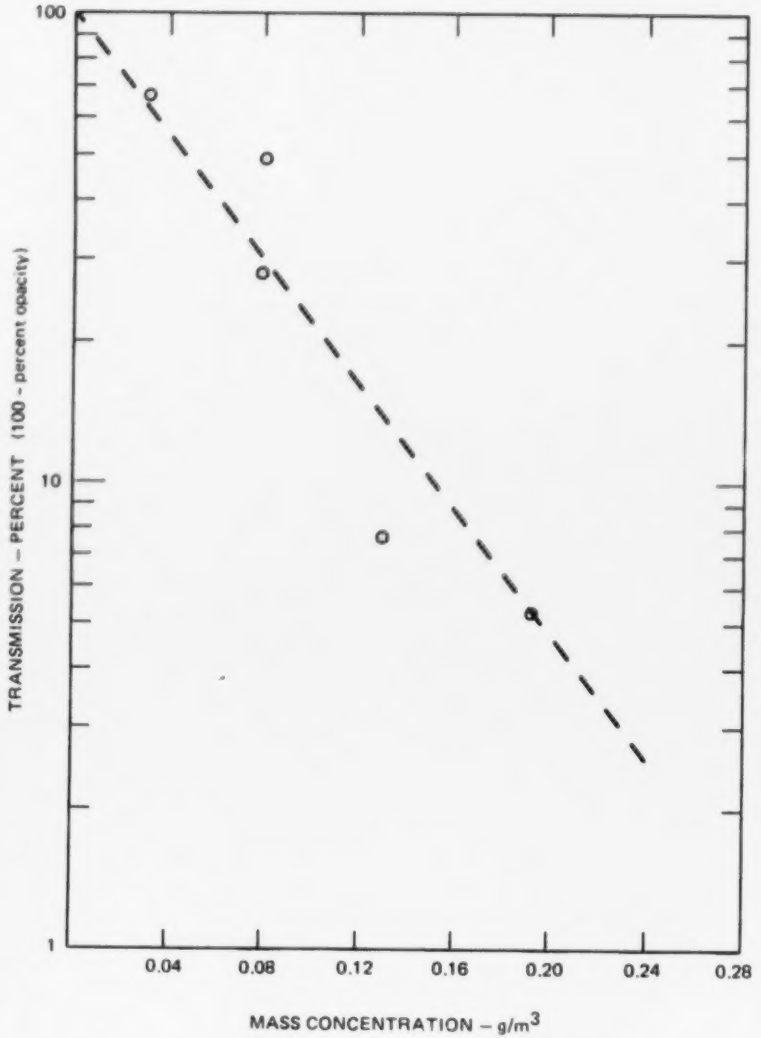

Figure 8. Calibration of CARB transmissometer in terms of aerosol mass concentration for white (diesel fuel) smoke.

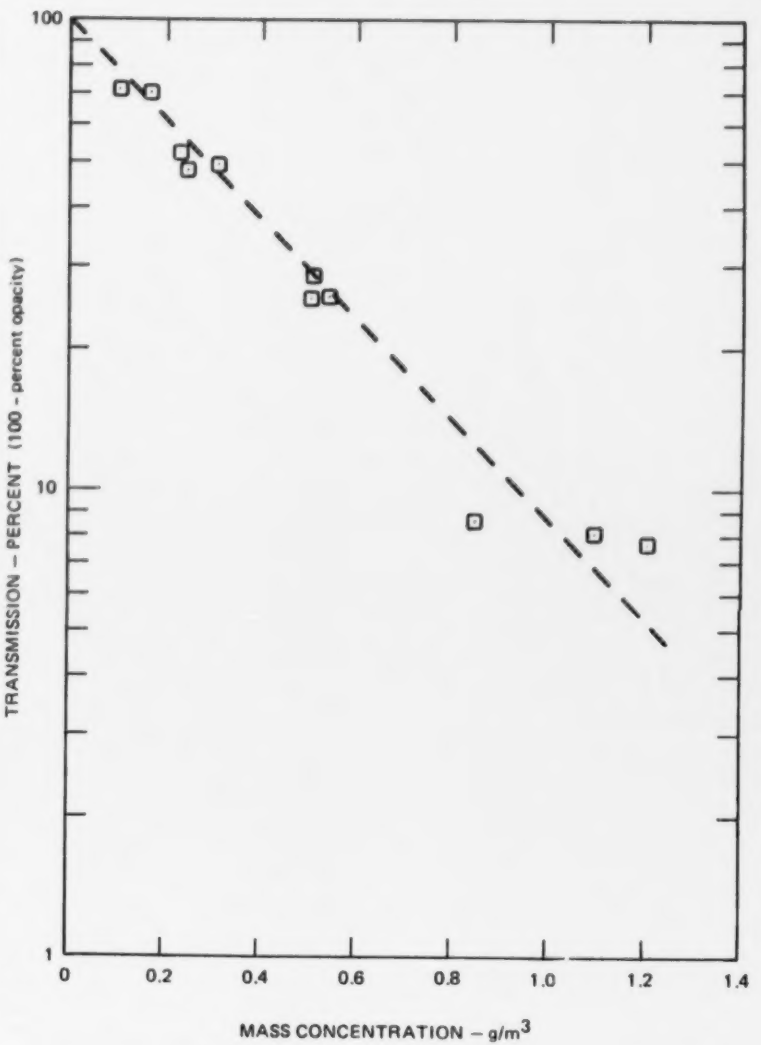

Figure 9. Calibration of CARB transmissometer in terms of aerosol mass concentration for black (toluene) smoke.

Black aerosol (incompletely combusted toluene) produced by the CARB smoke generator was emitted at rates of 3.3 to 28 g/min during the lidar field tests. The persistence of the submicron carbon particles downwind appeared to be good. Approximately 15 percent of the weight of toluene introduced to the generator was emitted as black smoke.

White Smoke (Pots and Candles)

Aerosol mass emission rates from the CARB smoke generator were determined to be smaller than desired, and a third aerosol was therefore produced from commercially available smoke pots and smoke candles. Zinc chloride smoke pots and candles were obtained from Superior Signal Co., Inc. Aerosols at various mass emission rates were produced by setting off 1, 2, 4, or 8 pots or candles simultaneously. Pots or candles were set off at heights of 15 ft, 3 ft, and ground level on a platform of a portable scaffold, as shown in Figure 10.

Since the aerosol generators for all cases were not portable, smoke production was delayed until favorable wind conditions were attained. Most of the tests were run in the late afternoon and early evening.

Emission Rates

Emission rates from smoke pots and candles were determined by measuring the mass concentration of aerosol in a 12-inch diameter stack as shown in Figure 11. The stack was 15-ft long and made of 12-inch diameter, 28-gauge galvanized heating duct. A 12-inch diameter, 16-gauge aluminum insert was secured in the top of the stack. The aluminum insert was fitted with a radius tap for measurement of the pressure drop across a 10-inch diameter sharp edged orifice attached to the top of the stack. Total airflow rates were determined by measuring the pressure drop across the orifice with a Magnehelic gauge.

The smoke pots and candles were placed in a 3-ft diameter wash tub directly under the vertical branch of the stack, and smoke was drawn into the stack by an ejector made of 3-inch diameter ABS pipe. Air was supplied to the ejector by a 1-hp centrifugal blower through the horizontal branch of the stack.

Filter samples were collected on 37-mm, 0.5-μm pore-size polyvinyl chloride (PVC) filters (manufactured by Mine Safety Appliances Co.) in closed-face filter cassettes. With these filters, sampling times of approximately 2 to 5 minutes were possible at a sampling rate of 2 l/min. Weights of the collected samples were from 10-20 percent of the filter tare weight. All samples were collected at the top of the stack shown in Figure 11.

Filter collection-efficiency measurements were made on the PVC filters by sampling with two filters in series. The average collection efficiency was 66 percent for the $ZnCl_2$ smokes, and all concentration measurements were corrected accordingly. Gravimeteric analyses in general were performed several days after actual sampling. Since the $ZnCl_2$ smoke is very hygroscopic, weight changes were detected on the filters as ambient humidity changed.

Figure 10. White smoke generation from pots and candles.

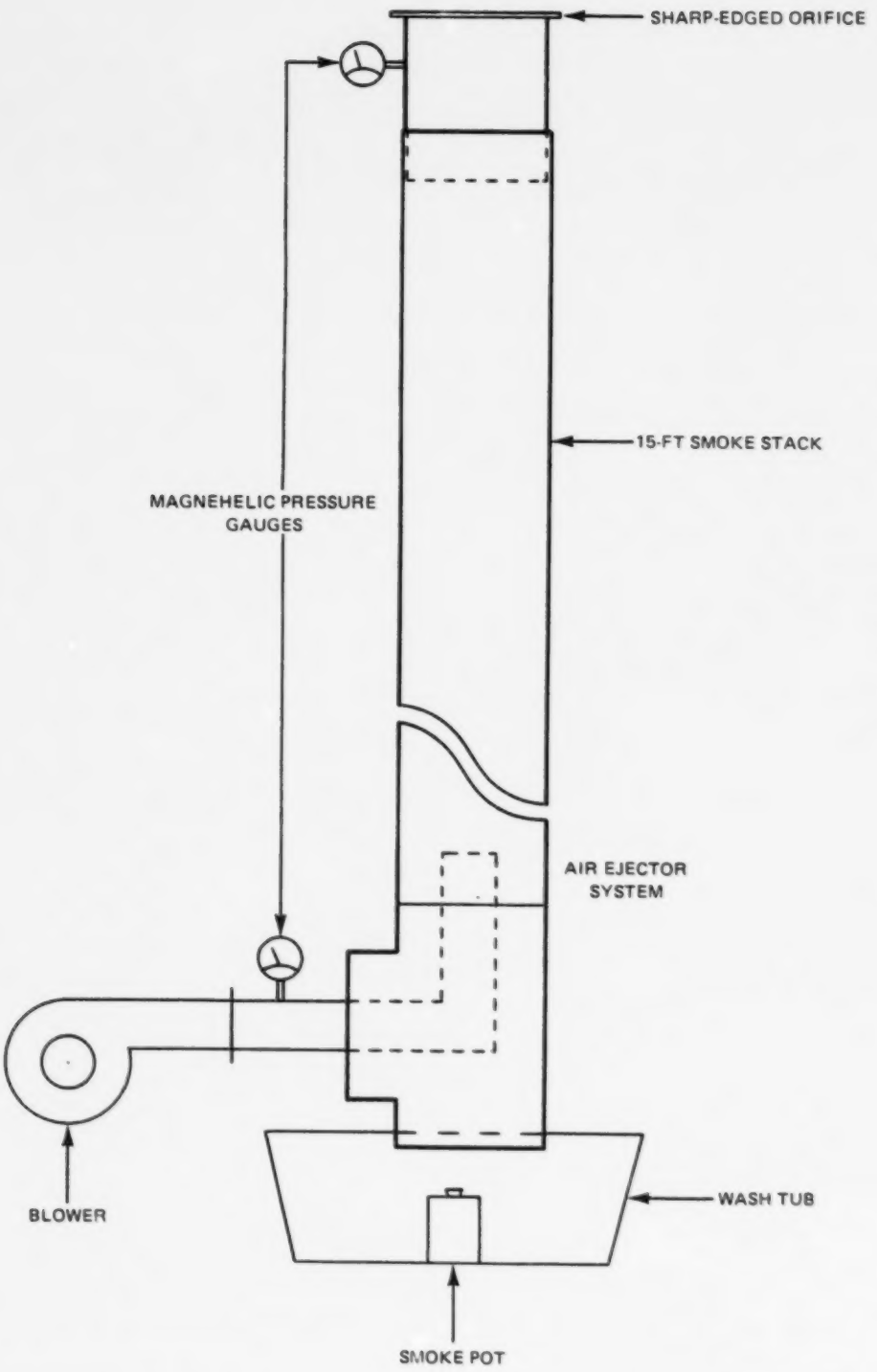

Figure 11. Method of evaluating aerosol mass concentration of emissions from smoke pots and candles.

Samples were therefore allowed to equilibrate at a relative humidity of about 60 percent before weighing.

Both pots and candles were used to generate aerosols of $ZnCl_2$. The only apparent difference between the pots and candles was the quantity of smoke emitted (the pots emitting roughly five times as much smoke as the candles).

The exact formulation of the pots and candles was not disclosed; however, military ZnCl smoke bombs are generally composed of aluminum, zinc oxide, and hexachloroethane. These components produce a grey smoke of $ZnCl_2$, Al_2O_3, and carbon. The smokes produced in the field were white and reported to be only $ZnCl_2$ and water by the manufacturer. $ZnCl_2$ is very hygroscopic, and each aerosol particle is reported to be about 50 percent absorbed or adsorbed water.

The aerosol mass output from the pots and candles (measured as described above) were somewhat variable. Output from a single pot or candle varied by as much as a factor of two, and the aerosol mass output rate from a pot or candle varied as much as a factor of four from the beginning to the end of a given smoke unit. For the most part, however, the average measured value of several pots or candles sampled one at a time appeared to be about one-half the value of those sampled two at a time. For this reason, it is probably that for those runs where more than a single smoke unit was set off (i.e., 2, 4, or 8 units), the mass emission rate was fairly consistent from test to test. The average output for a single smoke pot was about 45 g/min and for a single candle about 10 g/min. Thus, the range of aerosol mass emission rates for smoke pots was 45 to 360 g/min and for candles 10 to 80 g/min.

Aerosol Characterization

Field measurements of particle size for the $ZnCl_2$ smoke were made with a California Measurements piezoelectric cascade impactor. The instrument is basically a cascade impactor, which monitors, in close to real time, the amount of material collected. The impaction surfaces are oscillating piezoelectric crystals, which change oscillation frequency as material is deposited on them. Each collection stage holds two piezoelectric crystals. One crystal is the sampling crystal on which the particles are actually deposited. The other crystal is a reference crystal, which monitors the change in oscillation frequency in the sampling crystal. The impactor measures an aerodynamic diameter based on a density of 2.0 g/cc. Measurements were also made in the laboratory under controlled sampling conditions.

A log normal plot of the particle size distribution as measured in the laboratory is given in Figure 12. The aerodynamic mass median diameter of the $ZnCl_2$-H_2O aerosol is 1.1 μm, and the standard geometric deviation is about 2.86.

A summary of the smoke types and particle sizes used in this study is given in Table 3.

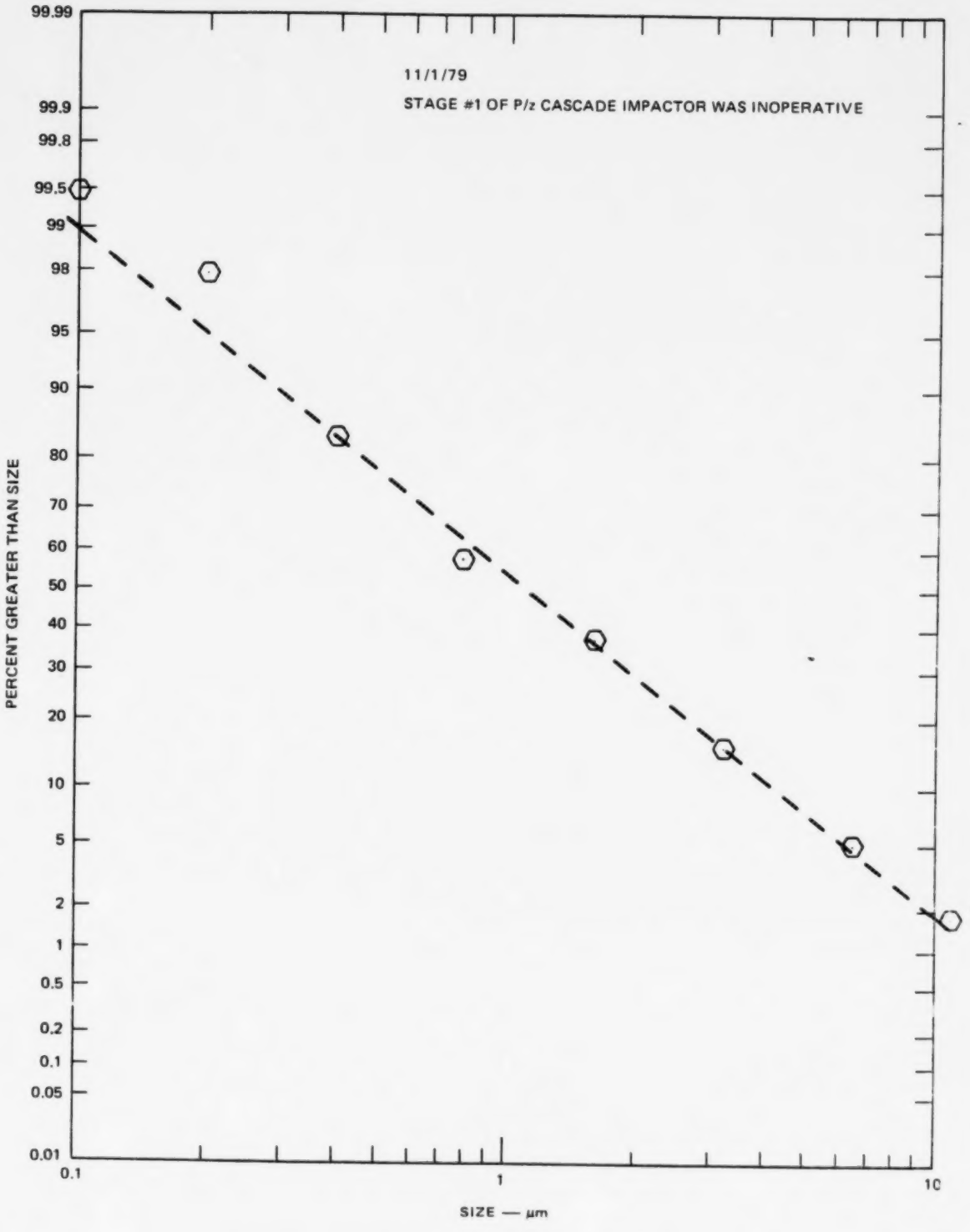

Figure 12. Particle size distribution smoke pots and candles

TABLE 3. AEROSOL CHARACTERISTICS

Aerosol Composition	Aerosol Type	Manufacturer	Range of Emission Rates Used (g/min)	Aerosol Mass Median Diameter (μm)
Silica	Powder (Min-U-Sil)	Pennsylvania Glass and Sand Co.	600-30,000	2.3*
Diesel fuel	White (Liquid)	CARB Smoke Generator	0.44-4.5	<1
Incompletely combusted toluene	Black (Carbon)	CARB Smoke Generator	3.3-28	<1
Zinc chloride + H_2O	Smoke pot	Superior Signal Smoke Co., Inc.	45-360	1.1
Zinc chloride + H_2O	Smoke candle	Superior Signal Smoke Co., Inc.	10-45	1.1

*Measured on another SRI project.

FIELD APPLICATION

Two experimental sites were used during the data collection program. The first site was located at Camp Parks, California. Only silica powder was used at Camp Parks during experiments that were conducted during May 1978 and again during September 1978. This field site was characterized by rolling hills: Resulting terrain features introduced problems with wind flow and complicated the lidar viewing geometry.

The Mark IX lidar was positioned 300 to 500 m from the source so that the laser beam would intersect the plume perpendicularly at a downwind distance of about 300 to 500 m. The lidar was scanned in elevation to observe the cross-plume aerosol distribution, similar to that shown in Figure 2. An anemometer was installed on the Mark IX lidar van, and its signal output was input to the lidar digital system so that both wind speed and direction were sampled for each lidar observation (firing). In addition, the output of an integrating nephelometer was similarly sampled. These data and the digital record of the backscatter signature were stored on magnetic tape for use during the data analysis program. For each experimental run, aerosol plumes were generated at three different particulate feed rates. For some meteorological conditions, the cross-plume aerosol density at a given distance from the source was quite variable. Therefore, a series of about 10 vertical lidar cross sections were collected for each particulate feed rate, so that a time-integrated cross-plume backscatter value could be evaluated.

The experimental procedure was reviewed during the September 1978 tests by the EPA Project Monitor, who suggested that further experiments be conducted at sites of both flat and complex terrain. He also suggested that alternative smoke sources may provide a more uniform particulate emission rate than was achieved with the dust feeder, and that other types of smoke would extend the general applicability of the lidar methodology.

A second series of experiments was scheduled to be conducted near Woodland, California, to collect a data base that would extend the general applicability of the lidar methodology. It was originally planned to conduct experiments using the CARB smoke generator at locations of flat and complex terrain. The experimental procedures were nearly identical to those used during the Camp Parks experiments; an additional element was the use of a trained smoke inspector to make smoke opacity readings during the lidar observations. Visual smoke readings were to be correlated with particulate emission rates and lidar observations.

During the first few days of the Woodland experiment (August 1979), it became obvious that the downwind plume density provided by the CARB smoke generator was not of sufficient density that satisfactory lidar observations could be made for a range of source emission rates. Some data were collected for black smoke, but no appropriate data were collected for white smoke because the smoke particles evaporated by the time the smoke reached the downwind distance viewed by the lidar. It was decided to replace the generator with smoke pots.

A supply of smoke pots was readily available at SRI. A scaffold was constructed so that the smoke could be emitted at heights up to 15 ft above the surface as shown in Figure 10. Aerosols of various emission rates were achieved by igniting 1, 2, 4, or 8 pots simultaneously. Although the method was successfully used and data for several runs were collected, the quantity of smoke was more than desired. For large smoke densities, attenuation of lidar backscattered energy becomes important. Cross-plume integrated backscatter uncorrected for attenuation would underestimate the smoke emission rate.

A supply of smoke candles, made by the manufacturer of the pots, was located and purchased. As discussed above, the smoke emission rate of the candles was determined to be about one-fifth of that for the smoke pots. The burn time was about 5 min, so about three lidar cross sections could be made during each test. Each test consisted of 1, 2, 4, or 8 candles burning simultaneously. Because of the additional effort required to modify the experimental approach to include smoke pots and candles, data were collected only at the flat-terrain site.

ANALYSIS METHOD

This section presents a method of processing the lidar data in terms of a quantity directly proportional to particulate emission rate. Range correction (see Eq. 1) was applied in real time by automatic adjustment of detector gain in a range-squared fashion. Resulting backscatter signatures were digitized in real time with a range interval of 1.5 m, and resulting data were stored on magnetic tape. The logarithmic lidar receiver was calibrated using neutral density filters. Figure 13 presents results of a typical calibration run indicating a linear relation between digitizer output (counts) and relative light input. The least-squares fit of the data points, shown as a dashed line in Figure 13, was used to compute light input from recorded records.

The range-dependent backscatter signatures were collected while the lidar was scanned in elevation to observe the total cross-plume aerosol (Figure 2). The integrated cross-plume backscatter was determined from the expression:

$$\int \beta_p \, dA = \int (\beta_p + \beta_c) \, dA - \int \beta_c \, dA' \left[\frac{\int dA}{\int dA'} \right] \quad , \tag{2}$$

where

β_p = plume backscatter coefficient [see Eq. (1)]

β_c = clear-air backscatter coefficient

A = area that includes all plume particulates

A' = area that excludes plume particulates.

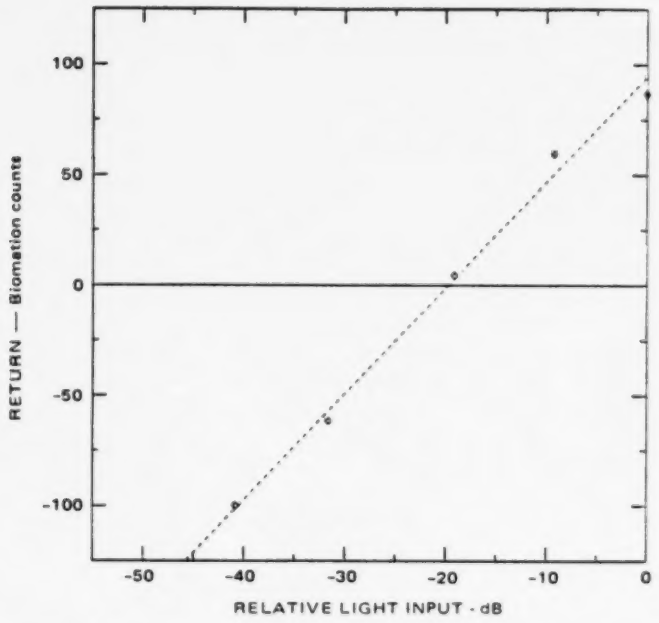

Figure 13. Mark IX laser calibration, Woodland, CA, 15 August 1979.

The first term represents plume and clear-air backscatter integrated over an area of the vertical cross section containing the plume, and the second term is an estimate of the clear-air backscatter integrated over the same area. Two different methods were used to evaluate Eq. 2. For the Camp Parks data, an objective method was applied to evaluate an array of backscatter values in Cartesian coordinates from the polar coordinate data records (Figure 2). The method, discussed by Uthe and Johnson (1980) consists of computing a backscatter value at each predetermined grid point based on data nearest to that point. The advantage of an x-y grid is that the resulting data array can easily be displayed with commonly used computer techniques to facilitate identification of plume and clear-air regions necessary to evaluate Eq. 2. For the Woodland data, Eq. 2 was evaluated in polar coordinate form. This method eliminates errors associated in transforming the polar coordinate data into an x-y grid. However, the plume values were not as easily inspected for determining plume and clear-air regions. For these data, the video displays produced by the Mark IX data system were used to evaluate proper integration intervals.

The primary objective of this study was to demonstrate experimentally that the integrated cross-plume backscatter responds in a linear manner to changes in the total mass concentration of particulate material released into the atmosphere. The total rate of fugitive dust emission, w, can be calculated from the distribution of particulate concentration in a given vertical plane downwind of the source by

$$w = \int cu \sin \theta \, dA \quad , \tag{3}$$

where c is the concentration in the area segment dA at which the wind velocity u is oriented at an angle θ to the vertical plane. Assuming c is proportional to the lidar backscatter coefficient ($c = k\beta$), and assuming a constant wind speed and direction at all parts of the vertical plane observed by the lidar, we have

$$w = Ku \sin \theta \int \beta_p \, dA \quad . \tag{4}$$

For each observation (vertical cross section), the backscatter records were processed in terms of an array of backscatter values for identifying appropriate clear-air and plume regions, to evaluate Eq. (2). The integrated cross-plume backscatter values were computed and statistically analyzed for the average and standard deviation for each set of observations made at a fixed particulate feed rate.

In addition to the analysis above, the smoke inspector readings made at the Woodland site were related to lidar cross-plume backscatter and independently evaluated smoke emission rates. The results of these analysis are presented in the following section of this report.

SECTION 5

RESULTS

Although results from both experimental programs are discussed below, the data base collected at Woodland is significantly more extensive than that collected at Camp Parks. Three different types of smoke were observed at Woodland, whereas only a single type was observed at Camp Parks. Smoke readings from a trained observer were made at Woodland, but not at Camp Parks. Therefore, the major analytical effort of this project was applied to the Woodland data base.

CAMP PARK RESULTS

At Camp Parks, ground silica particles were ejected into the atmosphere at heights of 1 and 10 m to form an aerosol plume observed by the lidar at a downwind distance of 300 to 500 m. Lidar signatures were integrated in the manner discussed in Section 4 to evaluate cross-plume backscatter. Figure 14 presents lidar evaluations related to independently determined particulate emission rates for two experimental runs. The cross-plume aerosol density at a given distance from the particulate source was quite variable, and therefore, a series of about 10 vertical lidar cross-sections were made at each particulate feed rate so that time-averages values of cross-plume backscatter could be determined. The average and ± one standard deviation values of integrated backscatter are shown in Figure 14.

Figure 14(a) presents experimental results using the integrated cross-plume backscatter as an estimate of the rate of fugitive dust emission. The data show that the integrated backscatter generally increases linearly with the particulate emission rate.

However, relatively large scatter of the data points occurs--i.e., large standard deviations--which can be explained partly on the basis of variable wind conditions that were ignored in this lidar derivation of emission rate.

Figure 14(b) presents the data shown in Figure 14(a) after corrections for observed wind-speed changes were applied; these were based on anemometer measurements made at the lidar site during the data-collection period. The wind corrections improve the linear relationship between the lidar observations and the particulate feed rates (especially for the second case), but the standard deviations remain about the same. The variability is thought to result partly from small-scale, uncontrolled variations in the particle feed rates and turbulent conditions, resulting in a nonuniform aerosol concentration downwind of the source. Both these factors were visually observed to

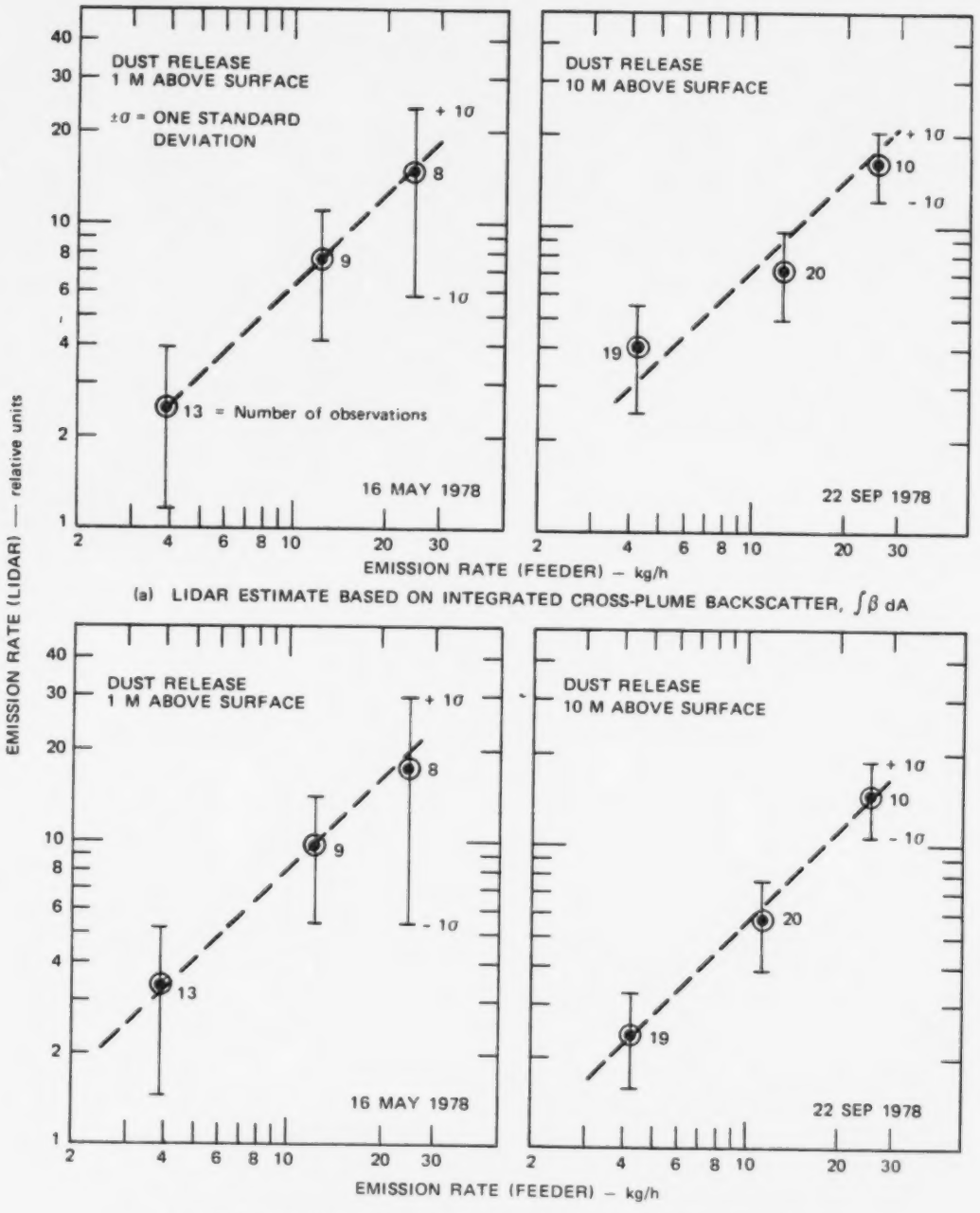
DUST RELEASE
1 M ABOVE SURFACE
±σ = ONE STANDARD DEVIATION
+ 1σ
- 1σ
13 = Number of observations
16 MAY 1978
DUST RELEASE
10 M ABOVE SURFACE
22 SEP 1978
EMISSION RATE (LIDAR) — relative units
EMISSION RATE (FEEDER) – kg/h
(a) LIDAR ESTIMATE BASED ON INTEGRATED CROSS-PLUME BACKSCATTER, ∫β dA
(b) LIDAR ESTIMATE BASED ON PRODUCT OF INTEGRATED CROSS-PLUME BACKSCATTER, A ∴ MEAN WIND SPEED, u∫β dA

Figure 14. Particulate emission rate evaluated from lidar, plotted as a function of emission rate as evaluated from the particle feeder.

Dashed line is the best-fit linear relation.

cause backscatter variations, but an estimate of their relative importance could not be made. Nevertheless, these data illustrate that the lidar technique provides a downwind measurement that responds in a predictable (linear) manner to the total particulate emission rate as evaluated from feeder calibration data. Based on these results, a more extensive experimental program was designed to extend the applicability of the lidar technique for measurement of fugitive particulate emissions. The results of the more extensive study are presented below.

WOODLAND RESULTS

At Woodland, California, experiments were conducted with black and white smoke generated from the CARB unit (Figure 7) and with smoke pots and candles (Figure 10). Details of smoke generation, experimental procedures, and data analysis methods were discussed in Section 4. Table 4 presents information on experimental times, geometry, smoke type, and smoke reader observations for the Woodland experiments. Results obtained for the black smoke, smoke pots, and smoke candles are presented below. Because most of the CARB white smoke evaporated along the downwind distance from the source to the point of lidar observation, results are not presented for this smoke type.

Black Smoke

Figure 15 presents lidar, emission, and smoke reader data collected during the 1805-1838 PDT period on 9 August 1979. Data tabulations are given in Appendix A. Figure 15(a) shows that the cross-plume integrated backscatter increases in a linear fashion with independently evaluated particulate emission rate. A linear squared correlation coefficient of $R_i^2 = 0.67$ ($R_i = 0.82$). is obtained between these observed quantities. Therefore, the linear relation, shown as a dashed line in Figure 15(a), explains 67 percent of the variance observed between these two quantities. The correlation between averaged values of lidar backscatter and emission rate is $R_m^2 = 0.97$. This large improvement in correlation using the mean values suggests that averaging multiple cross sections is required.

Figure 15(b) presents data relating cross-plume backscatter corrected for observed wind speed variations as a function of particulate emission rate. The particulate emission rate correlates slightly better with wind-corrected lidar backscatter ($R_i = 0.84$) than with uncorrected lidar backscatter ($R_i = 0.82$).

A trained smoke reader* made standard Method 9 visual observations of smoke opacity near the stack exit. Figure 15(c) indicates that transmission values (1 - opacity) from the visual observations follow a logarithmic relation with the wind-corrected cross-plume integrated backscatter, e.g., ln T

*Mr. R. Varner of the California Air Resources Board.

TABLE 4. LIDAR DATA LOG--SMOKE OBSERVATIONS
(Woodland, California, August 1979)

Date (1979)	Time (PDT)	Smoke Type*	Release Height† (m)	Downwind Viewing Direction (deg)	Lidar/Smoke Distance (m)	Downwind Distance (m)	Number of Lidar Cross-Sections	Opacity Smoke Reader (%)	Remarks
8 Aug	1650-1730	ARB-W	10	0	450	0	-	90, 70, 50, 30	Opacity runs over stack
	1800-1840	ARB-B	10	0	450	0	-	90, 70, 50, 30	Opacity runs over stack
	1850-1900	ARB-B	10	10	450	80	-		Smoke difficult to observe at downwind distances
9 Aug	1722-1732	ARB-W	10	5	300	30	5	30	50% Transmissometer
	1735-1743	ARB-W	10	5	300	30	4	35	30% Transmissometer
	1744-1752	ARB-W	10	5	300	30	3	70	90% Transmissometer
	1753-1757	ARB-W	10	5	300	30	3	60	70% Transmissometer
	1805-1811	ARB-B	10	5	300	30	4	50	50% Transmissometer
	1814-1821	ARB-B	10	5	300	30	5	80	70% Transmissometer
	1826-1831	ARB-B	10	5	300	30	3	90	90% Transmissometer
	1834-1838	ARB-B	10	5	300	30	3	40	30% Transmissometer
	1838-1842	ARB-B	10	21	380	150	3	40	30% Transmissometer
	1847-1852	ARB-B	10	21	380	150	3	90	90% Transmissometer
	1855-1900	ARB-B	10	21	380	150	3	50	50% Transmissometer
	1903-1910	ARB-B	10	21	350	130	4	75	70% Transmissometer
	1917-1922	ARB-W	10	21	350	130	3	85	90% Transmissometer
10 Aug	1641-1644	Clear Air					1		
	1646-1651	1P	5	20	320	120	3	45	1, 2, 4, 8 Smoke-pot runs
	1656-1701	2P	5	20	320	120	3	60-65	
	1711-1718	4P	5	20	320	120	4	60-70	
	1724-1731	8P	5	20	320	120	4	90	
	1738-1745	1P	5	30	380	220	4	20-25	
	1748-1754	2P	5	30	380	220	3	70	
	1759-1806	4P	5	30	370	210	4	75-80	
	1812-1818	8P	5	30	370	210	3	90	
	1827-1833	1P	1	30	350	200	3	40	
	1836-1840	2P	1	30	350	200	2	90	
	1845-1852	4P	1	30	350	200	4	80	
	1856-1902	8P	1	30	350	200	3	90	
	1910-1918	1P	0	30	350	200	4	30	
	1920-1926	2P	0	30	350	200	3	85	
	1929-1935	4P	0	30	350	200	3	95	

TABLE 4 (Concluded)

Date (1979)	Time (PDT)	Smoke Type*	Release Height (m)	Downwind Viewing Direction (deg)	Lidar/Smoke Distance (m)	Downwind Distance (m)	Number of Lidar Cross-Sections	Opacity Smoke Reader (%)	Remarks
15 Aug	1330-1350								Calibration
	1415-1440								Preliminary candle tests
	1445-1449	1C	5	30	450	260	2	10	Run with variable winds
	1452-1457	2C	5	30	450	260	3	20	
	1504-1508	4C	5	30	500	290	2	25	
	1521-1523	8C	5	30	450	260	1	50	
	1923-1927	1C	5	30	400	230	3	10	Run with uniform winds
	1928-1932	2C	5	30	350	200	3	20	
	1938-1942	4C	5	30	350	200	3	35	
	1946-1949	8C	5	30	350	200	3	50	
16 Aug	1500-1700								Installed new logger/calibration
	1702-1713	1P	5	30	320	180	4	30	Smoke-pot runs
	1717-1723	2P	5	30	330	180	3	50	
	1740-1745	4P	5	30	330	180	3	70	
	1752-1756	8P	5	30	340	200	3	90	
	1800-1820								Installed old logger/calibration
	1832-1836	1C	5	30	320	180	2	10	Smoke pot/candle comparisons
	1838-1845	1P	5	30	330	180	5	25	
	1847-1853	2C	5	30	350	200	3	20	
	1856-1902	2P	5	30	370	210	3	45	Road dust
	1908-1913	2P	5	30	400	230	3	55	Repeat run
	1935-1940	1C	1	30	450	260	3	20	
	1942-1948	2C	1	30	400	230	4	35	
	1950-1954	4C	1	30	450	260	4	75	
	1958-2008	8C	1	30	450	260	5	85	

*Key to smoke types:

ARB-W CARB smoke generator, white smoke, diesel fuel, submicron particle size, 30-300 g/h.

ARB-B CARB smoke generator, black smoke, incompletely combusted toluene, submicron size, 200-1700 g/h.

P Smoke pots, Superior Signal Co., white smoke, zinc chloride + H_2O, 0.25-μm particle size, 2,700-21,600 g/h.

C Smoke candles, Superior Signal Co., white smoke, zinc chloride + H_2O, 0.3-μm particle size, 600-4800 g/h.

†Smoke emission rates are given in the Appendix.

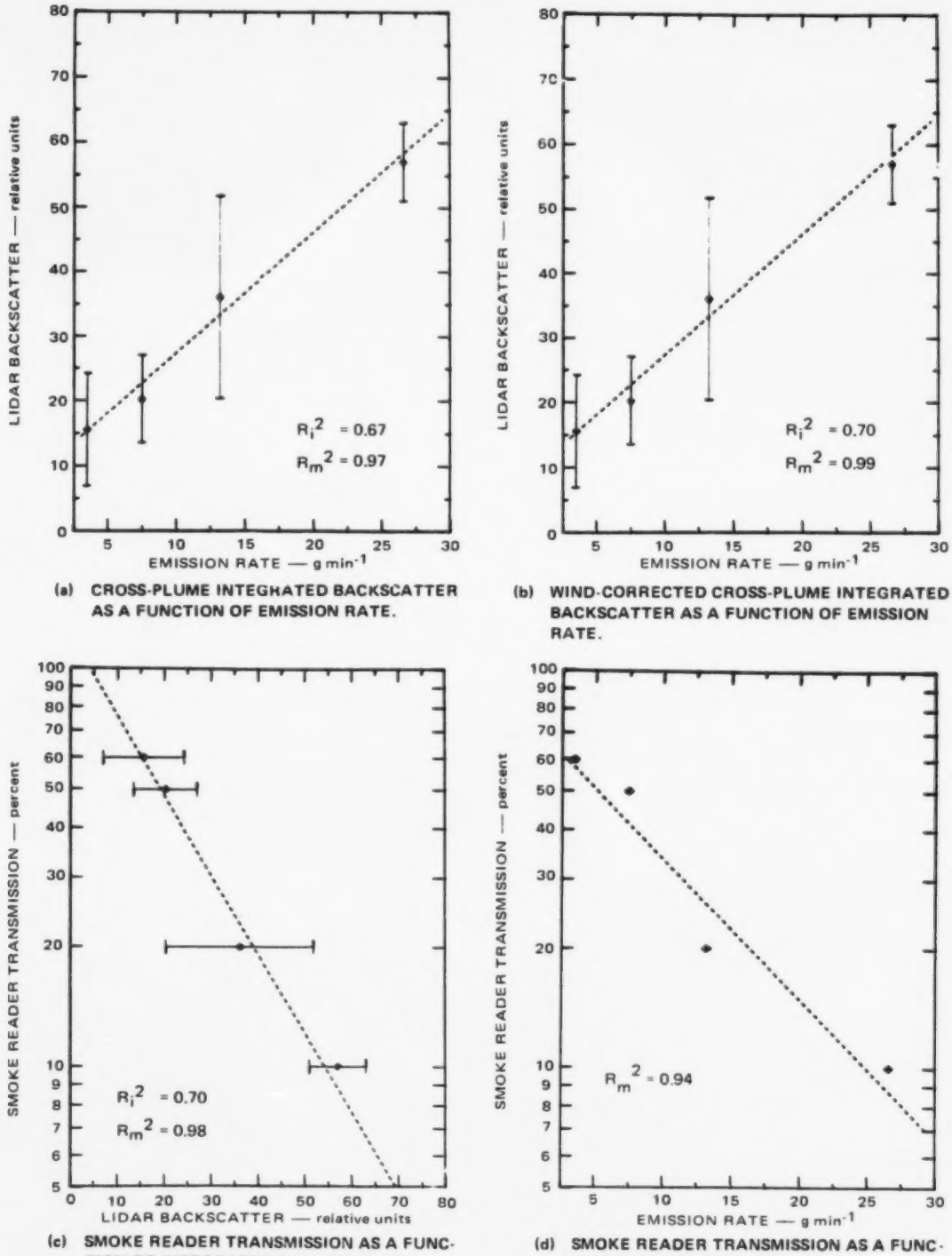
LIDAR BACKSCATTER — relative units
EMISSION RATE — g min-1
Ri2 = 0.67
Rm2 = 0.97
LIDAR BACKSCATTER — relative units
EMISSION RATE — g min-1
Ri2 = 0.70
Rm2 = 0.99
SMOKE READER TRANSMISSION — percent
LIDAR BACKSCATTER — relative units
Ri2 = 0.70
Rm2 = 0.98
SMOKE READER TRANSMISSION — percent
EMISSION RATE — g min-1
Rm2 = 0.94

(a) CROSS-PLUME INTEGRATED BACKSCATTER AS A FUNCTION OF EMISSION RATE.

(b) WIND-CORRECTED CROSS-PLUME INTEGRATED BACKSCATTER AS A FUNCTION OF EMISSION RATE.

(c) SMOKE READER TRANSMISSION AS A FUNCTION OF INTEGRATED BACKSCATTER.

(d) SMOKE READER TRANSMISSION AS A FUNCTION OF EMISSION RATE.

Figure 15. Lidar, emission, and smoke reader data for CARB black smoke (9 August 1979, 1805–1838 PDT).

10-m release height, 15 lidar cross sections.

is proportional to - β dA. This result may have been expected from the following expressions:

- $\ln T = - \sigma dl$ (Bouger's law of attenuation with T = transmission and σ = volume extinction coefficient).
- $\beta \propto \sigma$ (Backscatter is proportion to extinction).
- $\int \beta \, dl \propto \int \beta \, dA$ (Backscatter integrated along the observer's viewing direction is proportional to the cross-plume integrated backscatter).

Therefore, the data imply that the plume density integrated along the path viewed by the observer is proportional to the cross-plume integrated density. For the case of the black smoke, the visual readings were made near the stack exit; these terms are expected to be well correlated because variation of the cross-plume geometry near the stack is small.

Figure 15(d) shows that the logarithm of the observer transmission values is linearly related to the smoke emission rate, w. This follows from data presented in Figure 15(b), showing that cross-plume integrated backscatter is linearly related to particulate emission rate, and from data presented in Figure 15(c), indicating that the cross-plume integrated backscatter is linearly related to the logarithm of transmission as evaluated by visual observations. The cross-plume backscatter and visual (transmission) observations are well correlated, because the plume geometry does not vary greatly at the stack exit. The higher correlation of the smoke reader's values with emission rate than with lidar backscatter was expected since the emission measurements were made within the stack, the reader observations were made just over the stack, and the lidar measurements were made 30-m downwind of the stack.

Figure 16 presents data collected for black smoke on 9 August, 1838 to 1910 PDT. While the lidar backscatter is well correlated with particulate emission rate, the constant of proportionality is substantially different from that for the data presented in Figure 15. This indicates that another influencing factor must be accounted for in order to estimate particulate emission rate from cross-plume integrated backscatter. Inspection of Table 4 shows that the lidar viewing angle was changed between data collection runs in order to observe the plume at a greater downwind distance from the source. Therefore, changes in the downwind characteristics of the smoke plume may have affected the results of this experiment.

As shown in Figure 16(c) and (d), the smoke-observer-evaluated transmissions are well correlated with the cross-plume backscatter and particulate emission rate. The relationship between transmission and emission rate is nearly identical to that of the earlier data run [Figure 15(d)], while the relationship between transmission and cross-plume backscatter is substantially different from that observed on the earlier data run [Figure 15(c)]. This indicates that changing the lidar viewing direction caused the factor-of-two increase in observed cross-plume backscatter. Such a large increase cannot be explained by increased path lengths through the plume at the larger downwind distance. Rather, increased backscatter indicates increased plume

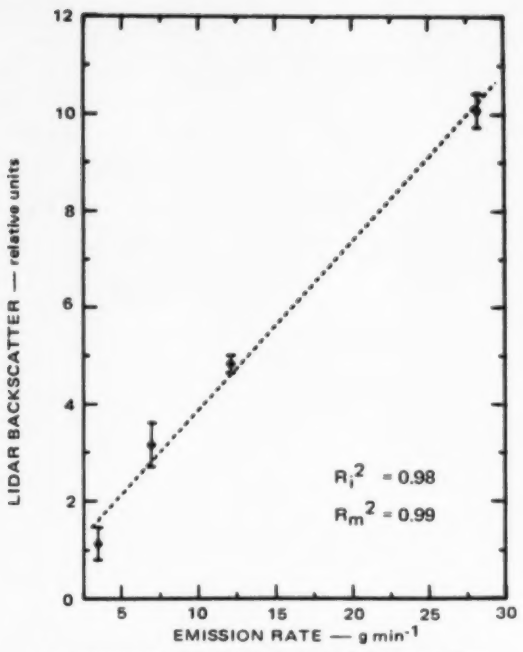

(a) CROSS-PLUME INTEGRATED BACKSCATTER AS A FUNCTION OF EMISSION RATE.

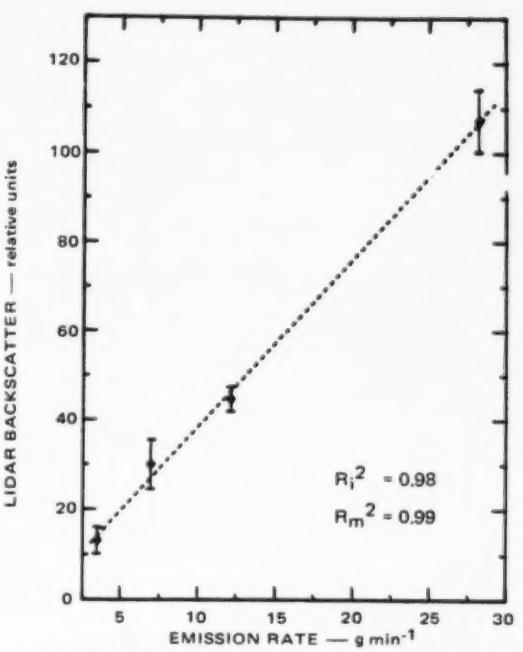

(b) WIND-CORRECTED CROSS-PLUME INTEGRATED BACKSCATTER AS A FUNCTION OF EMISSION RATE.

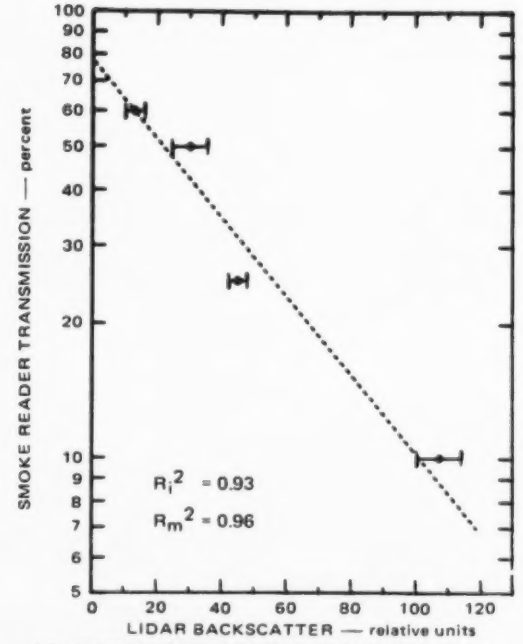

(c) SMOKE READER TRANSMISSION AS A FUNCTION OF INTEGRATED BACKSCATTER.

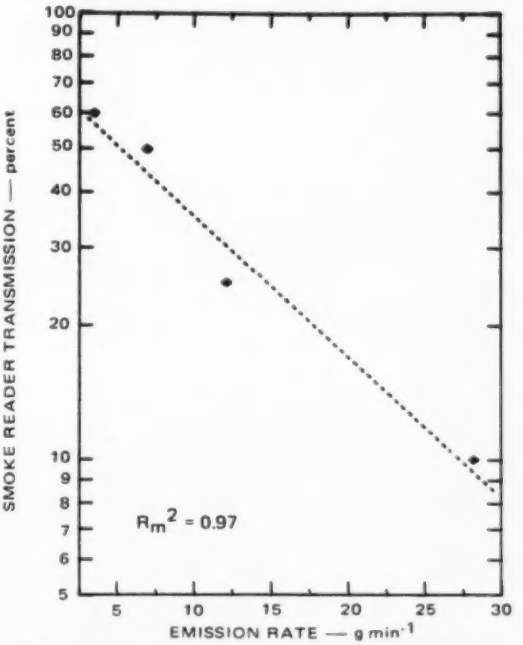

(d) SMOKE READER TRANSMISSION AS A FUNCTION OF EMISSION RATE.

Figure 16. Lidar, emission, and smoke reader data for CARB black smoke (9 August 1979, 1838–1910 PDT).

10-m release height, 13 lidar cross sections.

density downwind of the source. This is consistent with visual observations that the downwind plume could be characterized in three distinct zones of behavior with each zone containing a different cross-plume density. The near-stack zone resembled a jet plume--a horizontal well-defined plume with little vertical extent. The plume then underwent a turbulent transition, with the plume well defined but with large vertical movement. The final stage of development was a well-mixed plume which appeared lower in horizontal velocity, resulting in increased aerosol density. This appearance could have resulted as the plume mixed downward toward the surface while wind speed decreased with lower elevation.

Although the data shown in Figures 15 and 16 were collected in a slightly different manner, it is interesting to combine these results for black smoke as shown in Figure 17. The mean values of the lidar observations for different emission rates follow a linear relation with emission rate ($R_m^2 = 0.99$). Moreover, the linear relation is nearly 1 to 1, e.g., as the emission rate increases by a factor of 2, the integrated cross-plume backscatter increases by a factor of 2. Correlation of the smoke reader data with smoke emission rate is significantly higher than with the integrated cross-plume backscatter. This is expected, as the smoke reader made his observations near the stack rather than at the downwind distance being observed by the lidar.

Smoke Pots

A series of experiments were conducted with commercially available smoke pots in order to generate a greater quantity of smoke than could be produced with the CARB smoke generator. The method of smoke release and characterization of particle size and emission rate were discussed in Section 4. During the smoke pot experiments, the smoke reader made his observations at a downwind plume distance corresponding to that being observed by the lidar. Therefore, a lower correlation between smoke reader transmission and measured emission rate is expected than for the case of the black smoke, for which the smoke reader made his observations just over the stack, e.g., standard Method 9 observations. However, a higher correlation between the smoke reader and lidar data is also expected.

Lidar, emission, and smoke reader data for three experimental periods are shown in Figures 18, 19, and 20. These data generally show the expected relationships between the observations. The largest correlations are obtained for data presented in Figure 19, with substantially smaller correlation between observed quantities for data presented in Figures 18 and 20. In addition, the best-fit linear relation (dashed line) between integrated backscatter and particulate emission rate is nearly a one-to-one relation for the data shown in Figure 19, but not for the data shown in Figures 18 and 20. The smoke reader observations are also substantially better correlated with lidar and smoke emission values for data presented in Figure 19 than for data presented in Figures 18 and 20.

Similar wind direction and speeds were recorded for the three smoke pot tests; however, as shown by Table 4, the experimental conditions were slightly different for each run. For the first run (Figure 18), smoke was

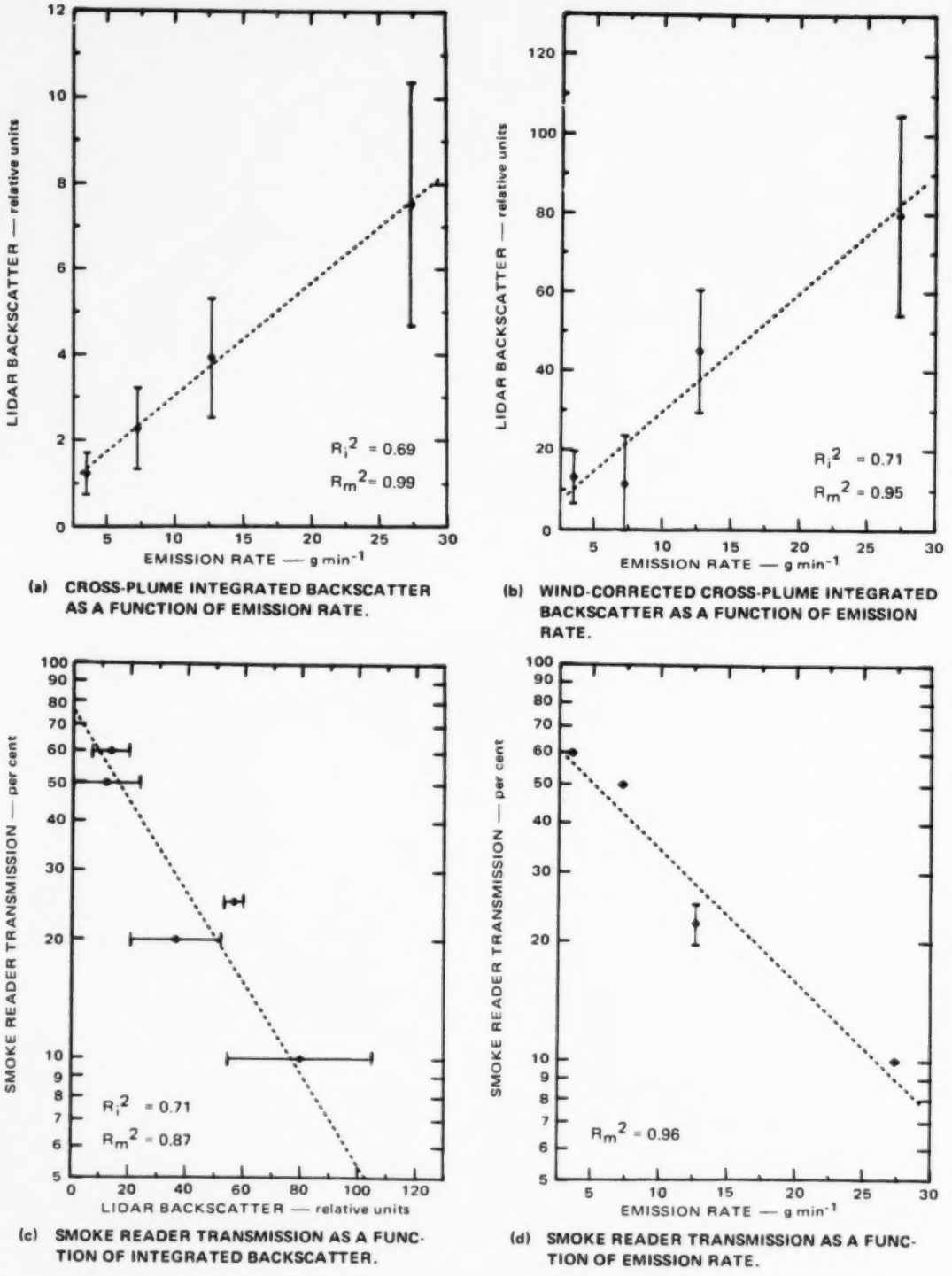
LIDAR BACKSCATTER — relative units
EMISSION RATE — g min-1
Ri2 = 0.69
Rm2 = 0.99
(a) CROSS-PLUME INTEGRATED BACKSCATTER AS A FUNCTION OF EMISSION RATE.
LIDAR BACKSCATTER — relative units
EMISSION RATE — g min-1
Ri2 = 0.71
Rm2 = 0.95
(b) WIND-CORRECTED CROSS-PLUME INTEGRATED BACKSCATTER AS A FUNCTION OF EMISSION RATE.
SMOKE READER TRANSMISSION — per cent
LIDAR BACKSCATTER — relative units
Ri2 = 0.71
Rm2 = 0.87
(c) SMOKE READER TRANSMISSION AS A FUNCTION OF INTEGRATED BACKSCATTER.
SMOKE READER TRANSMISSION — per cent
EMISSION RATE — g min-1
Rm2 = 0.96
(d) SMOKE READER TRANSMISSION AS A FUNCTION OF EMISSION RATE.

Figure 17. Lidar, emission, and smoke reader data for CARB black smoke (combined runs). 10-m release height, 28 lidar cross sections.

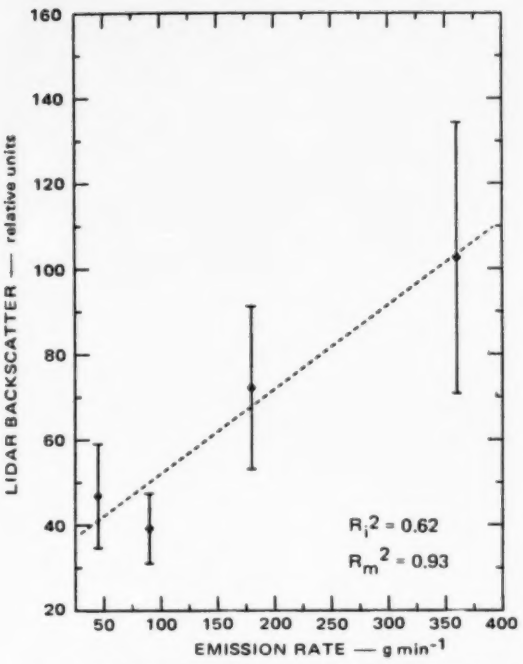

(a) CROSS-PLUME INTEGRATED BACKSCATTER AS A FUNCTION OF EMISSION RATE.

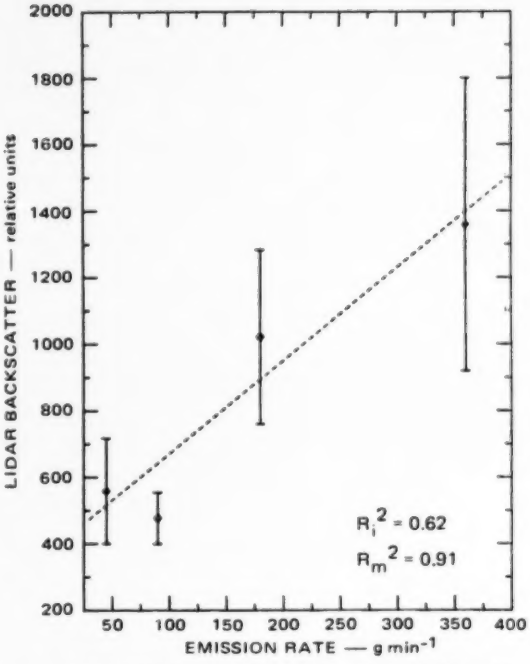

(b) WIND-CORRECTED CROSS-PLUME INTEGRATED BACKSCATTER AS A FUNCTION OF EMISSION RATE.

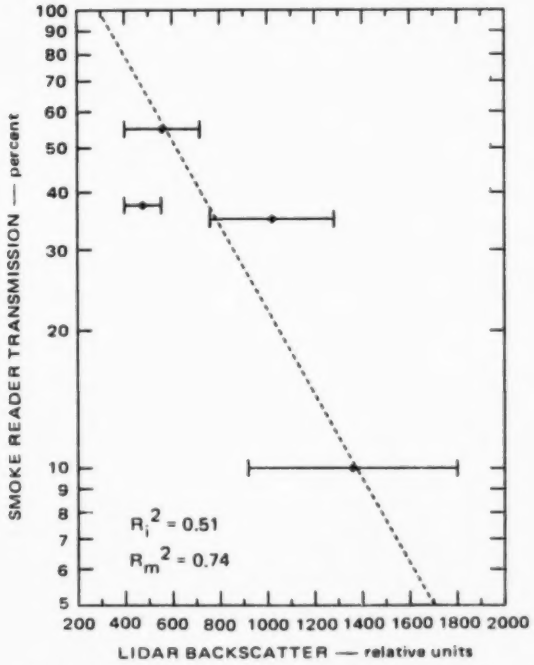

(c) SMOKE READER TRANSMISSION AS A FUNCTION OF INTEGRATED BACKSCATTER.

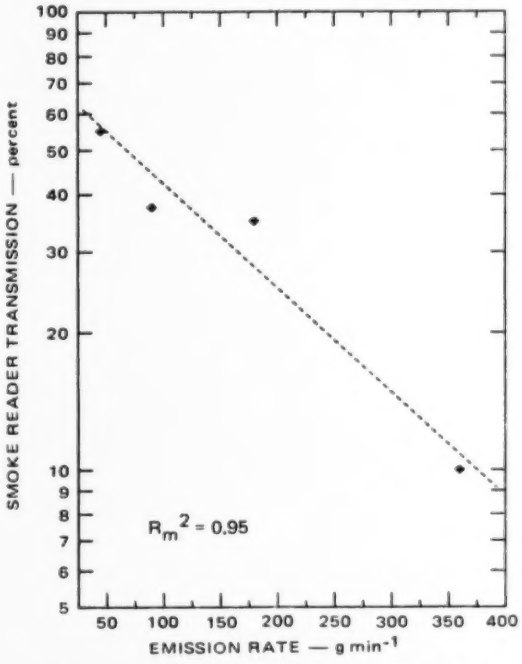

(d) SMOKE READER TRANSMISSION AS A FUNCTION OF EMISSION RATE.

Figure 18. Lidar, emission, and smoke reader data for smoke pots (10 August 1979, 1646–1731 PDT). 5-m release height, 14 lidar cross sections.

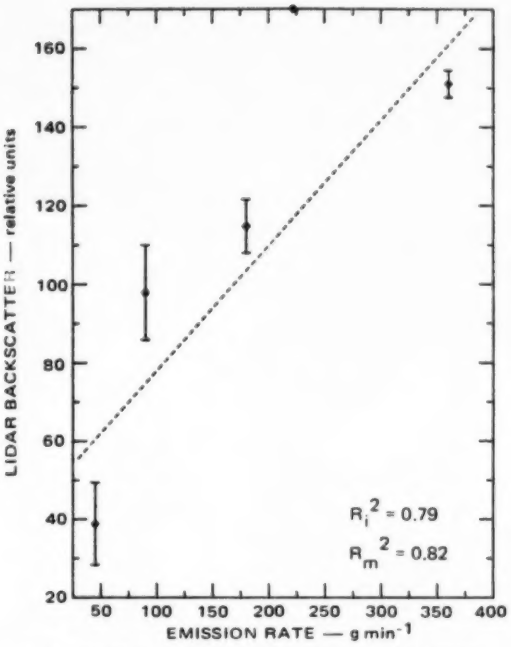

(a) CROSS-PLUME INTEGRATED BACKSCATTER AS A FUNCTION OF EMISSION RATE.

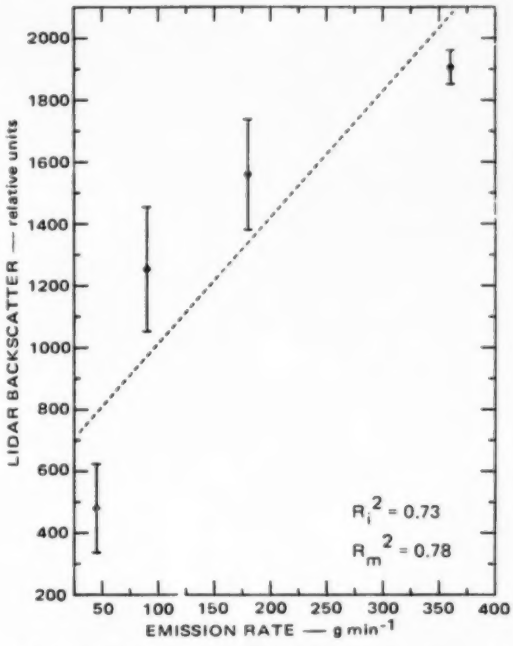

(b) WIND-CORRECTED CROSS-PLUME INTEGRATED BACKSCATTER AS A FUNCTION OF EMISSION RATE.

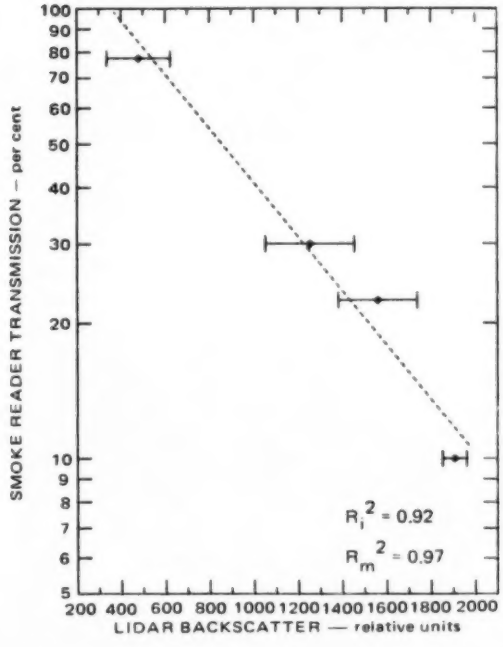

(c) SMOKE READER TRANSMISSION AS A FUNCTION OF INTEGRATED BACKSCATTER.

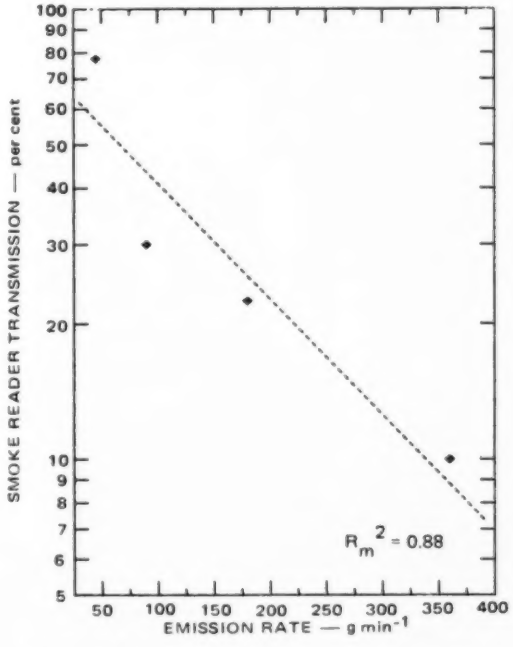

(d) SMOKE READER TRANSMISSION AS A FUNCTION OF EMISSION RATE.

Figure 19. Lidar, emission, and smoke reader data for smoke pots (10 August 1979, 1738–1818 PDT). 5-m release height, 14 lidar cross sections.

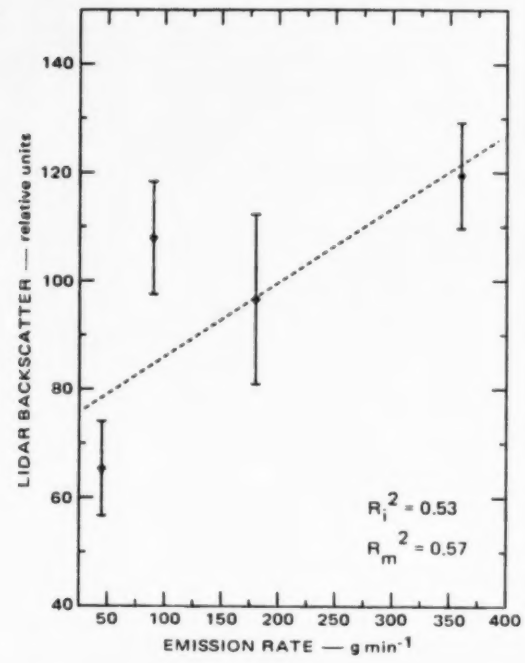

(a) CROSS-PLUME INTEGRATED BACKSCATTER AS A FUNCTION OF EMISSION RATE.

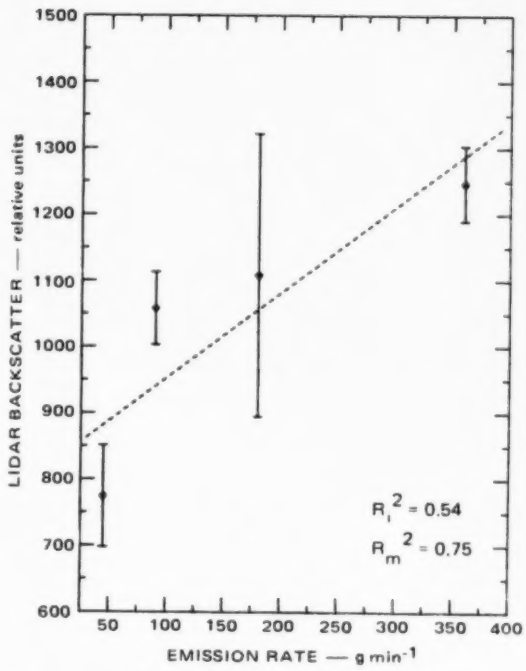

(b) WIND-CORRECTED CROSS-PLUME INTEGRATED BACKSCATTER AS A FUNCTION OF EMISSION RATE.

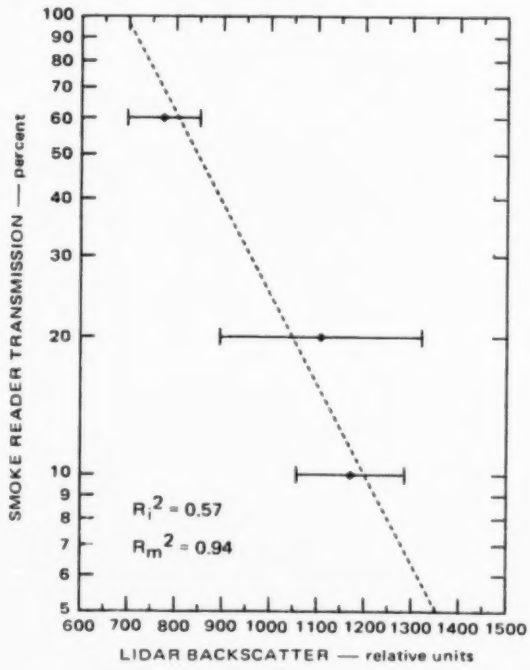

(c) SMOKE READER TRANSMISSION AS A FUNCTION OF INTEGRATED BACKSCATTER.

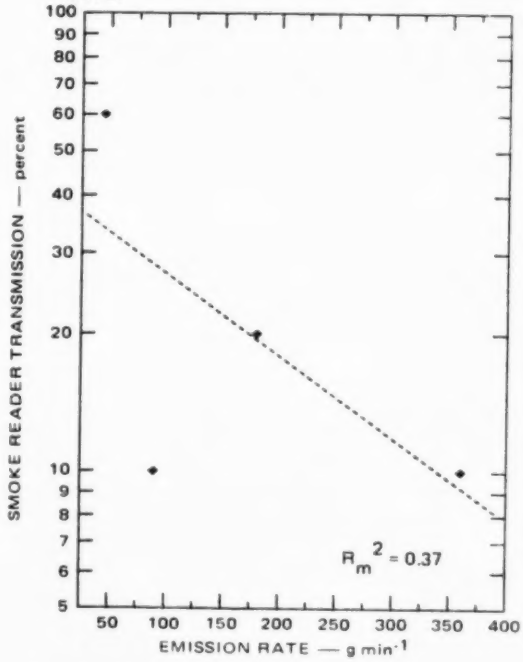

(d) SMOKE READER TRANSMISSION AS A FUNCTION OF EMISSION RATE.

Figure 20. Lidar, emission, and smoke reader data for smoke pots (10 August 1979, 1827–1902 PDT). 1-m release height, 12 lidar cross sections.

released from a height of 5 m and the lidar observed the smoke about 120 m downwind of the source. For the second data run (Figure 19) the lidar observed the smoke at a farther downwind distance (220 m). For the third data run, the lidar viewed the smoke at the farther downwind distance, but the smoke release was only 1 m above ground level. The results of the smoke pot tests indicate that higher correlation is obtained between integrated cross-plume backscatter and particulate emission rate for smoke released from higher elevation and for lidar viewing at greater downwind distances. This conclusion is consistent with visual observations that the plume was spatially more uniform in density at greater downwind distances and that smoke released from low levels impacted on the surface and therefore had a higher probability of undergoing density changes during its downwind transport.

Figure 21 presents the lidar, emission, and smoke reader data combined for the three smoke pot experiments. The mean values of integrated backscatter observed at each particulate emission rate are linearly related to emission rate ($R_m^2 = 0.91$). However, the best-fit linear relation is substantially different from a one-to-one relationship, e.g., a factor of two increase in particulate emission produced less than a factor of two increase in lidar integrated backscatter. The smoke produced by the smoke pots was very dense, and attenuation of the laser energy by the smoke particles probably reduced observed backscatter for larger emission rates by the amount indicated in Figure 21(a) and (b). The data presented in Figure 21(c) and 21(d) indicate that trained observer readings of downwind smoke concentrations provide useful information on the source strength, i.e., particulate emission rate.

Smoke Candles

The experimental procedure used during the smoke pot experiments appeared to provide suitable data on lidar response to increasing particulate emissions. However, the pots produced such a high-density smoke that the relationship between cross-plume integrated backscatter and particulate emission rate was affected by attenuation of the laser energy by the smoke particles (see Eq. 1). In order to produce a smoke plume of lesser density (while retaining the experimental procedure used with the smoke pots), SRI obtained a supply of smoke candles. Lidar, emission, and smoke reader data for two experimental runs with smoke candles are shown in Figures 22 and 23. These two experiments were conducted on different days and with different smoke release heights (5 m and 1 m) but with the same experimental procedure as used with the smoke pots.

The results presented in Figure 22 show a high correlation among the backscatter, smoke reader, and emission data (R_m^2 values of 0.95 and higher). The correlation between mean values of cross-plume integrated backscatter and particulate emission rate was not improved when the backscatter values are corrected for observed wind-speed variations [Figure 22(b)]. However, the correlation between individual values was improved, indicating wind correction is not needed with data averaging. Unlike the case of the smoke pots, the best-fit linear expression here approximates a one-to-one relation. The lidar backscatter values (average) and the smoke reader data correlate

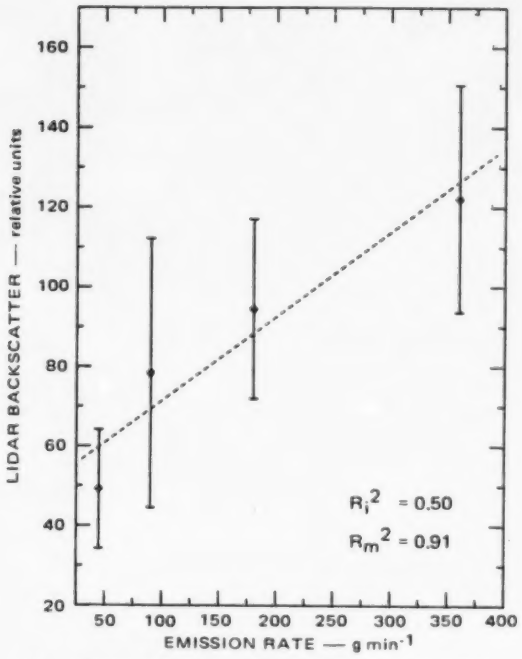

(a) CROSS-PLUME INTEGRATED BACKSCATTER AS A FUNCTION OF EMISSION RATE.

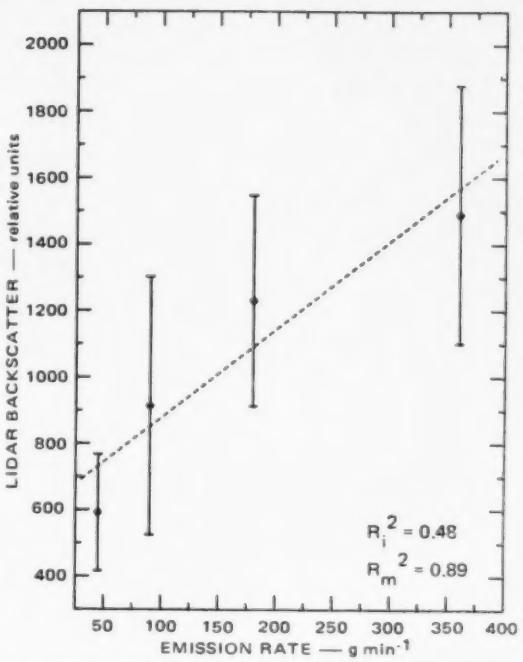

(b) WIND-CORRECTED CROSS-PLUME INTEGRATED BACKSCATTER AS A FUNCTION OF EMISSION RATE.

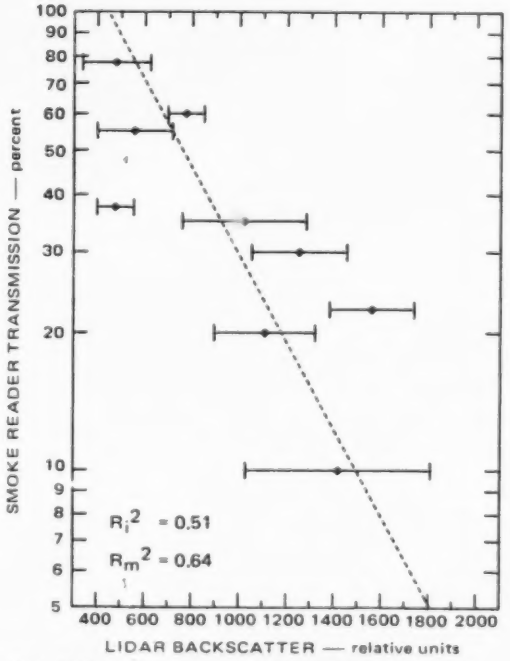

(c) SMOKE READER TRANSMISSION AS A FUNCTION OF INTEGRATED BACKSCATTER.

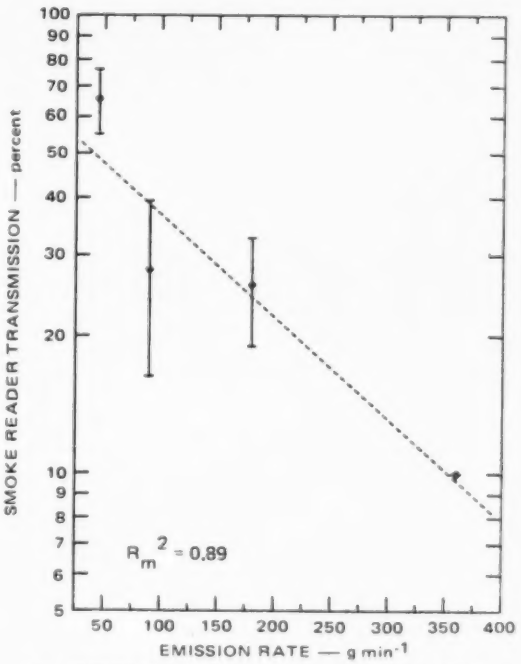

(d) SMOKE READER TRANSMISSION AS A FUNCTION OF EMISSION RATE.

Figure 21. Lidar, emission, and smoke reader data for smoke pots (combined data).

40 lidar cross sections.

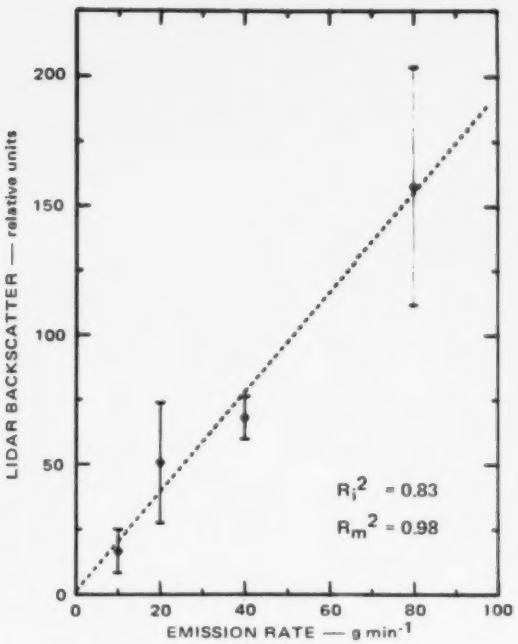

(a) CROSS-PLUME INTEGRATED BACKSCATTER AS A FUNCTION OF EMISSION RATE.

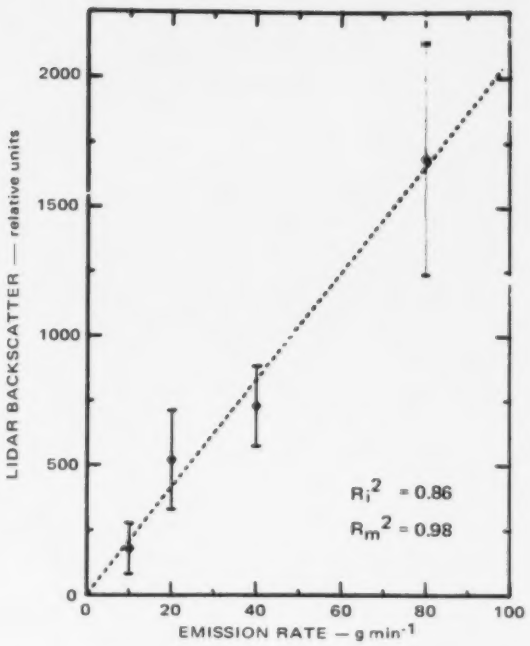

(b) WIND-CORRECTED CROSS-PLUME INTEGRATED BACKSCATTER AS A FUNCTION OF EMISSION RATE.

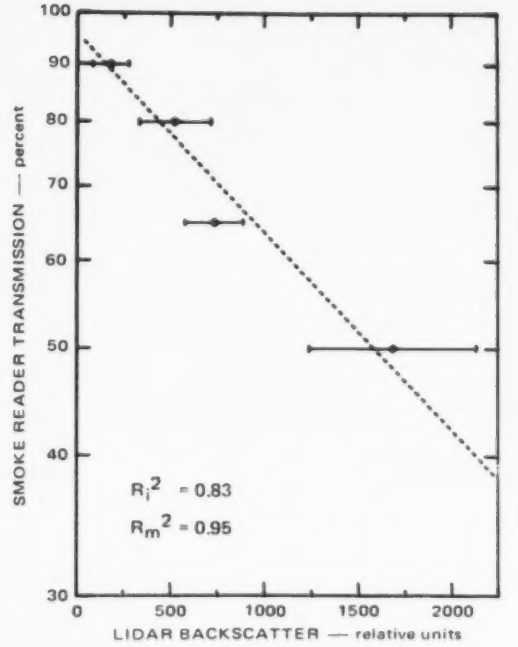

(c) SMOKE READER TRANSMISSION AS A FUNCTION OF INTEGRATED BACKSCATTER.

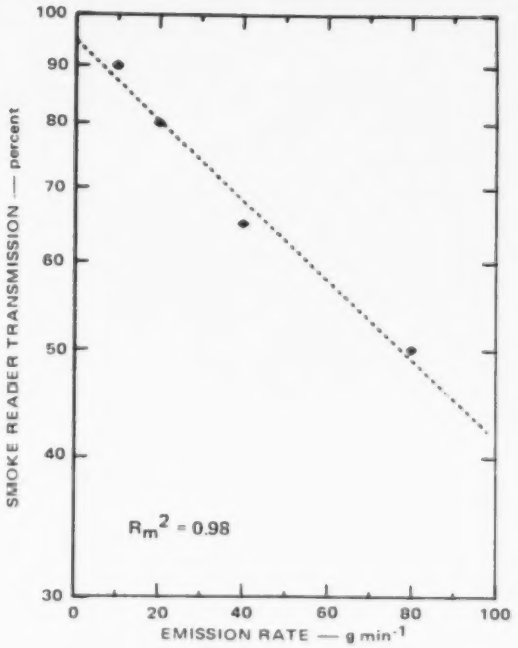

(d) SMOKE READER TRANSMISSION AS A FUNCTION OF EMISSION RATE.

Figure 22. Lidar, emission, and smoke reader data for smoke candles (15 August 1979, 1923–1949 PDT).

5 m release height, 12 lidar cross sections.

equally well with smoke emission rate. This imples that the cloud geometry along the path observed by the smoke reader remained constant during the data collection. This result also suggests that a modified Method 9 approach used for observer reading of plume opacity of stationary source emissions may be useful for reading opacity downwind of emissions from fugitive emission sources.

The data presented in Figure 23 for smoke released at a height of 5 m are similar to those presented in Figure 22 for release at a height of 1 m. Correcting the lidar observations for observed wind-speed variations decreases correlation with smoke emission, but the correlation was slightly increased in the case of the 5-m release. As was the case for the smoke pots, correlation between observer readings and particulate emission is lower for smoke released at 1 m than at 5 m.

Figure 24 presents lidar, emission and smoke reader data obtained by combining results presented in Figures 22 and 23 with the smoke candle data collected on 16 August during 1832-1853 PDT (see Table 4). The average lidar readings at each of the four particulate emissions (1, 2, 4, and 8 candles) are related nearly linearly on a one-to-one basis with emission rate. Correcting the lidar observations by observed wind speed variations decreases correlation of individual values between the lidar observations and particulate emission but has no effect on mean values. The relatively low correlation of individual smoke observer readings with lidar and emission values for combined data was expected, as the cloud geometry was observed to depend on smoke release height (see Eq. 5).

Correlation Summary

Table 5 presents a summary of squared linear-correlation coefficients evaluated between parameters observed at Woodland. Cross-plume integrated backscatter is relatively well correlated with particulate emission for all data collected. Correction for wind speed variations slightly improves the correlation of individual values but not mean values. The correlation between the lidar and emission data is not obviously dependent on smoke release height. The correlations are generally higher for data derived during a single data collection period than for data combined for all experimental periods, which indicates other influencing factors not accounted for in the measurement program.

Correlation of lidar data with observer data is very similar to the correlation of lidar data with emission data. Again, correction for observed wind speed variations has virtually no effect on the correlation values.

Lidar-Derived Opacities

Plume opacities may be derived from the lidar backscatter records for comparison with the smoke reader observations. The technique is to determine opacity by comparing the backscatter from the clear-air regions before and after the plume return (Cook et al., 1972; Evans, 1967). Lidar-derived plume opacities for a smoke pot run (eight pots) are shown in Figure 25(a). Each

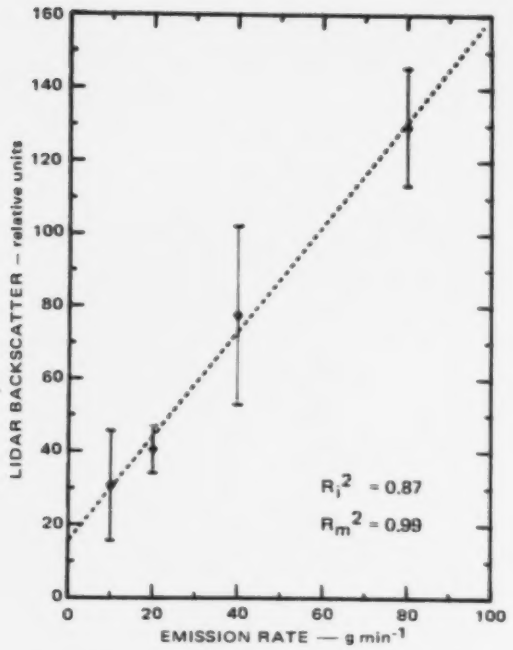

(a) CROSS-PLUME INTEGRATED BACKSCATTER AS A FUNCTION OF EMISSION RATE.

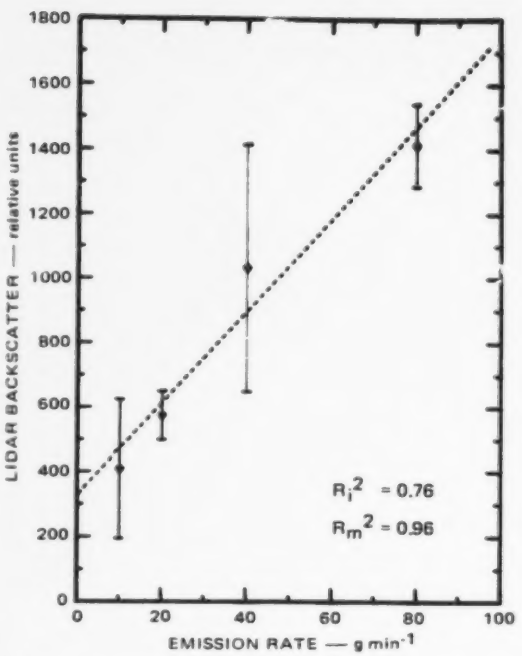

(b) WIND-CORRECTED CROSS-PLUME INTEGRATED BACKSCATTER AS A FUNCTION OF EMISSION RATE.

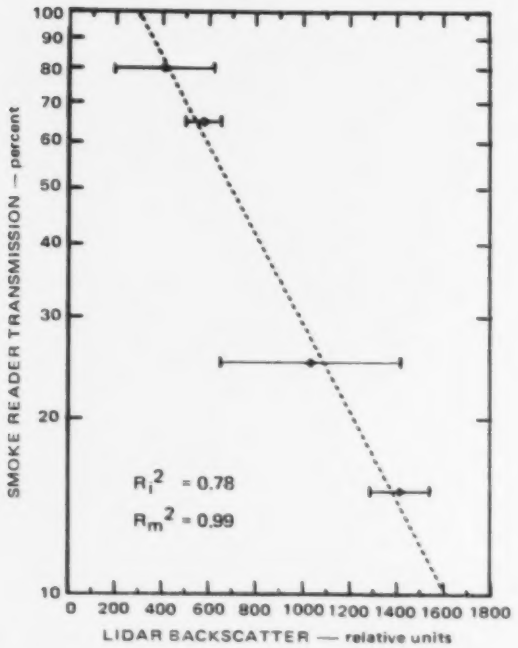

(c) SMOKE READER TRANSMISSION AS A FUNCTION OF INTEGRATED BACKSCATTER.

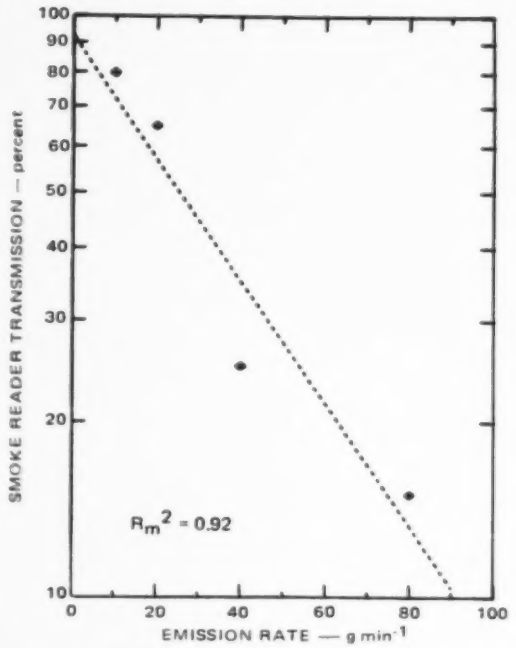

(d) SMOKE READER TRANSMISSION AS A FUNCTION OF EMISSION RATE.

Figure 23. Lidar, emission, and smoke reader data for smoke candles (16 August 1979, 1935–2008 PDT).

1 m release height, 15 lidar cross sections.

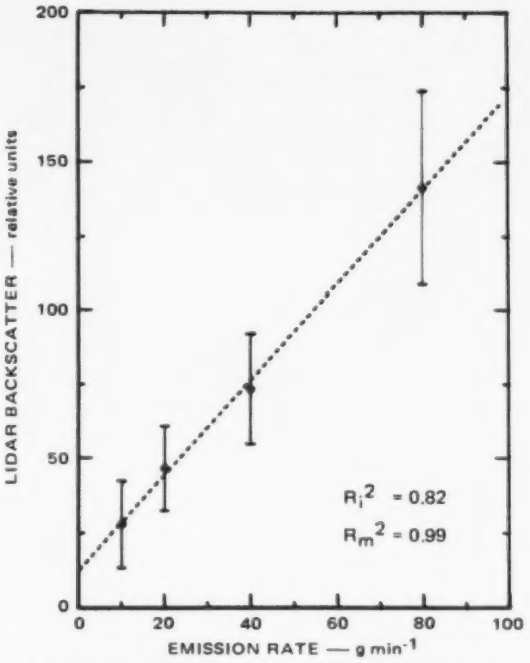

(a) CROSS-PLUME INTEGRATED BACKSCATTER AS A FUNCTION OF EMISSION RATE.

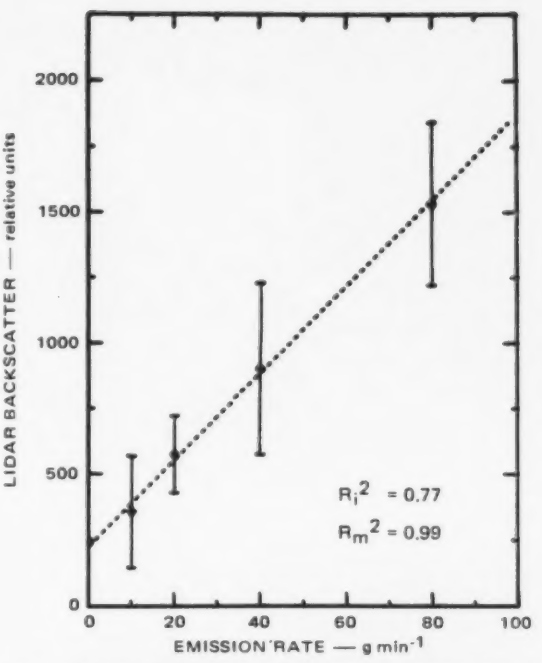

(b) WIND-CORRECTED CROSS-PLUME INTEGRATED BACKSCATTER AS A FUNCTION OF EMISSION RATE.

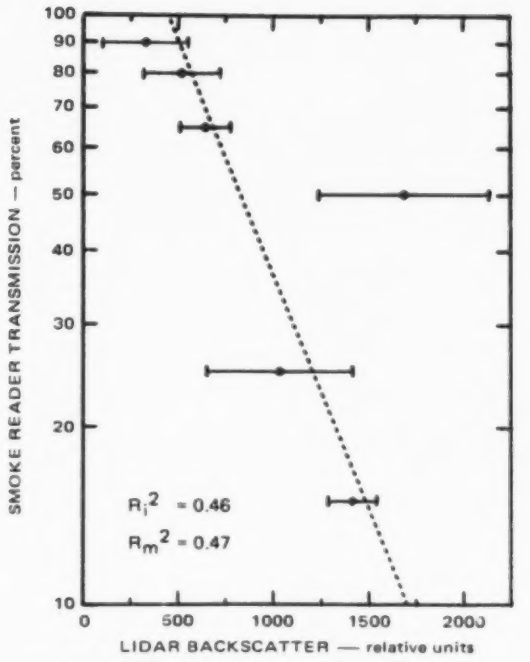

(c) SMOKE READER TRANSMISSION AS A FUNCTION OF INTEGRATED BACKSCATTER.

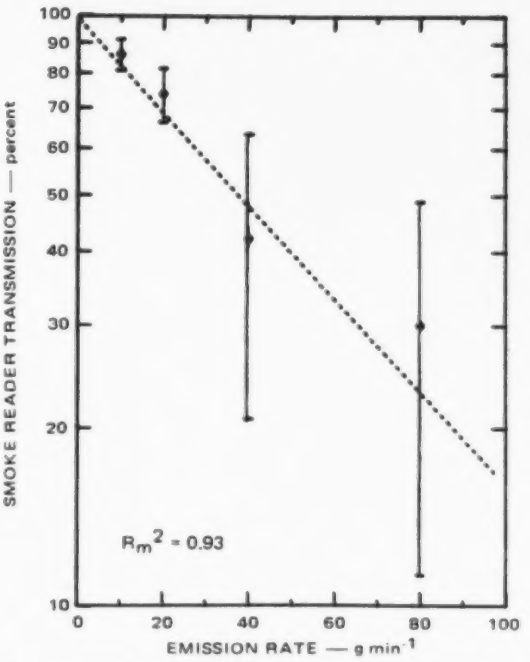

(d) SMOKE READER TRANSMISSION AS A FUNCTION OF EMISSION RATE.

Figure 24. Lidar, emission, and smoke reader data for smoke candles (combined data, all runs). Data for combined 1 and 5m release heights, 32 lidar cross sections.

TABLE 5. LINEAR CORRELATION COEFFICIENTS SQUARED (R^2)

Smoke Type	Date	Release Height (m)	Time (PDT)	Lidar Scans	Emission Rates	R_i^2 (Individual Points)*				R_m^2 (Means)†				
						$\int\beta\, dA/ER$‡	$\bar{u}\int\beta\, dA/ER$	$\int\beta\, dA/\ln T_{SR}$	$\bar{u}\int\beta\, dA/\ln T_{SR}$	$\int\beta\, dA/ER$	$\bar{u}\int\beta\, dA/ER$	$\int\beta\, dA/\ln T_{SR}$	$\bar{u}\int\beta\, dA/\ln T_{SR}$	$\ln T_{SR}/ER$
ARB-B	9 Aug	10	1805-1838	15	4	0.67	0.70	0.69	0.70	0.97	0.99	0.99	0.98	0.94
	9 Aug	10	1838-1910	13	4	0.98	0.98	0.96	0.93	0.99	0.99	0.97	0.96	0.97
	Total	--		28	4	0.69	0.71	0.63	0.71	0.99	0.95	0.85	0.87	0.96
Smoke	10 Aug	5	1646-1731	14	4	0.62	0.62	0.53	0.51	0.93	0.91	0.80	0.74	0.95
Pots	10 Aug	5	1738-1818	14	4	0.79	0.73	0.96	0.92	0.82	0.78	0.99	0.97	0.88
	10 Aug	1	1827-1902	12	4	0.53	0.54	0.77	0.57	0.57	0.75	0.99	0.94	0.37
	Total	--		40	4	0.50	0.48	0.64	0.51	0.91	0.89	0.74	0.64	0.89
Candles	15 Aug	5	1923-1949	12	4	0.83	0.86	0.81	0.83	0.98	0.98	0.94	0.95	0.98
	16 Aug	5	1832-1853	5	2	0.20	0.06	0.20	0.06	-§	-§	-§	-§	-§
	16 Aug	1	1935-2008	15	4	0.87	0.76	0.83	0.78	0.99	0.96	0.95	0.99	0.92
	Total	--		32	4	0.82	0.77	0.42	0.46	0.99	0.99	0.40	0.47	0.93

Symbols: $\int\beta\, dA \equiv$ Cross-plume integrated lidar backscatter

$ER \equiv$ Smoke emission rate

$\ln T_{SR} \equiv$ Natural logarithm of smoke reader transmission

$\bar{u} \equiv$ Mean wind speed

*R^2 computed using all individual data points

†R^2 computed using dependent variable means for a given independent variable value

‡Dependent/independent variable

§R^2 = 1 for these cases but has no meaning because there are only two data points

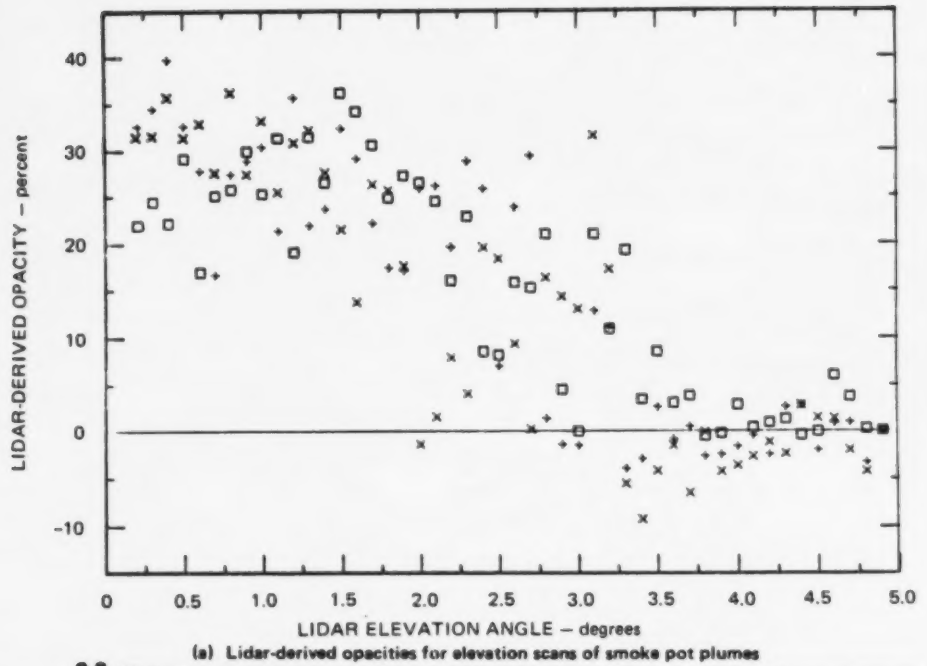

(a) Lidar-derived opacities for elevation scans of smoke pot plumes

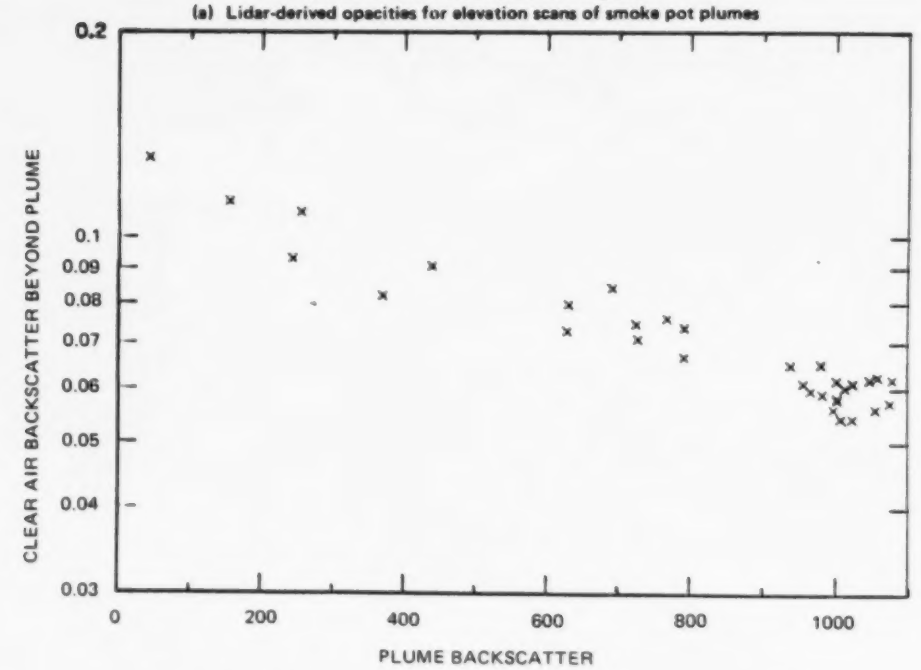

(b) Clear-air backscatter beyond plume as a function of plume backscatter

Figure 25. Lidar opacity analysis for smoke pot plumes.

data point is derived from one lidar signature, and points of the same symbol were made during an elevation scan; therefore, these data give a vertical distribution of plume opacity. The values are substantially less than the 90-percent reading made by the smoke inspector. The air at Woodland was exceptionally clean with little clear-air backscatter observed by the lidar (lidar operation was optimized for plume observation, rather than clear-air observation). Therefore, for high-density plumes, the backscatter from the far side of the plume may have approached the noise level of the lidar receiver, thereby limiting the density of plumes for which opacity could be determined. Figure 25(b) plots the clear-air return beyond the plume return as a function of the plume backscatter. As indicated by this data plot, the clear-air return beyond the plume did not saturate with respect to the plume backscatter; therefore, the lidar opacity values should be valid.

The Mark IX lidar system transmits laser energy at a wavelength of 0.6943 μm, and the spectral response of the smoke observer is maximum at a wavelength of about 0.53 μm. Therefore, depending on the size of the scattering particles, the opacity evaluated by the lidar, O_R, will underestimate that evaluated by the smoke observer, O_G. Conner and White (1980) have corrected ruby lidar opacity measurements by the expression:

$$O_G = 1 - (1 - O_R)^{Q_G/Q_R} \quad ,$$

where Q_G/Q_R is the ratio of extinction coefficients at green and red wavelengths. Because of the small size of the smoke particles (see Section 4) a value of 2.0 can be assumed for Q_G/Q_R, and corrected maximum lidar opacities O_G of about 60 percent are obtained. This value is substantially less than the 90 percent value reported by the smoke inspector. This result may indicate that the smoke reader was biased by the large size of the downwind smoke plume. It should be noted that the visual observations of white smoke (smoke pots) were made against a clear sky background, with a single tree the only distant dark object within view. For these less-than-ideal viewing conditions, an error of 30 percent in opacity was possible. It is also possible that the smoke reader's eye followed dense smoke patches that escaped detection by the lidar. The correlation of lidar-derived opacities with observer opacities was not a major task of this study, and the above-noted discrepancy was not investigated further.

SECTION 6

OBSERVATIONS AT A FUGITIVE EMISSIONS SOURCE

A final task of this project was to demonstrate the use of the lidar technique at the site of an actual fugitive emissions source. The purpose was not to estimate particulate emission from the source, but rather to show that a lidar system can be used to collect the necessary backscatter data for this purpose.

The Mark IX mobile lidar used on the earlier stages of this project was operated near the site of the Permanente Cement Plant located in Cupertino, California. This site is characterized by particulate emissions from stacks as well as from bag-house and truck hauling operations. Truck hauling operations conducted during dry weather periods are a major cause of particulate loading downwind of the source.

On 21 May 1980, the lidar van was positioned about 2 km from the plant, and a series of lidar elevation scans were made in an azimuth direction such that the particulate plume was observed about 500 m downwind of the plant, as shown in Figure 26. The backscatter signatures were used to generate intensity-modulated displays of plume structure, as shown in Figure 27 for six elevation scans. The center of the pollution plume is about 1.9 km from the lidar, and the plume extended to about 400 m in elevation. The lidar pulses impacted on a hill about 3 km from the lidar (Figure 26), resulting in the black area surrounded by white in the lower right-hand side of the lidar cross sections. The returns above the hill resulted from a dense fog that was penetrating from the far side of the hill.

The method of data collection at Permanente was nearly identical to the method of data collection used at Woodland during the observation of controlled particulate emissions. Therefore, the backscatter returns from the Permanente pollution plume could be integrated using the same technique discussed in Section 4 and used to obtain the results presented in Section 5. The results of this study demonstrate that the lidar technique is applicable for the measurement of particulate emissions from actual fugitive sources.

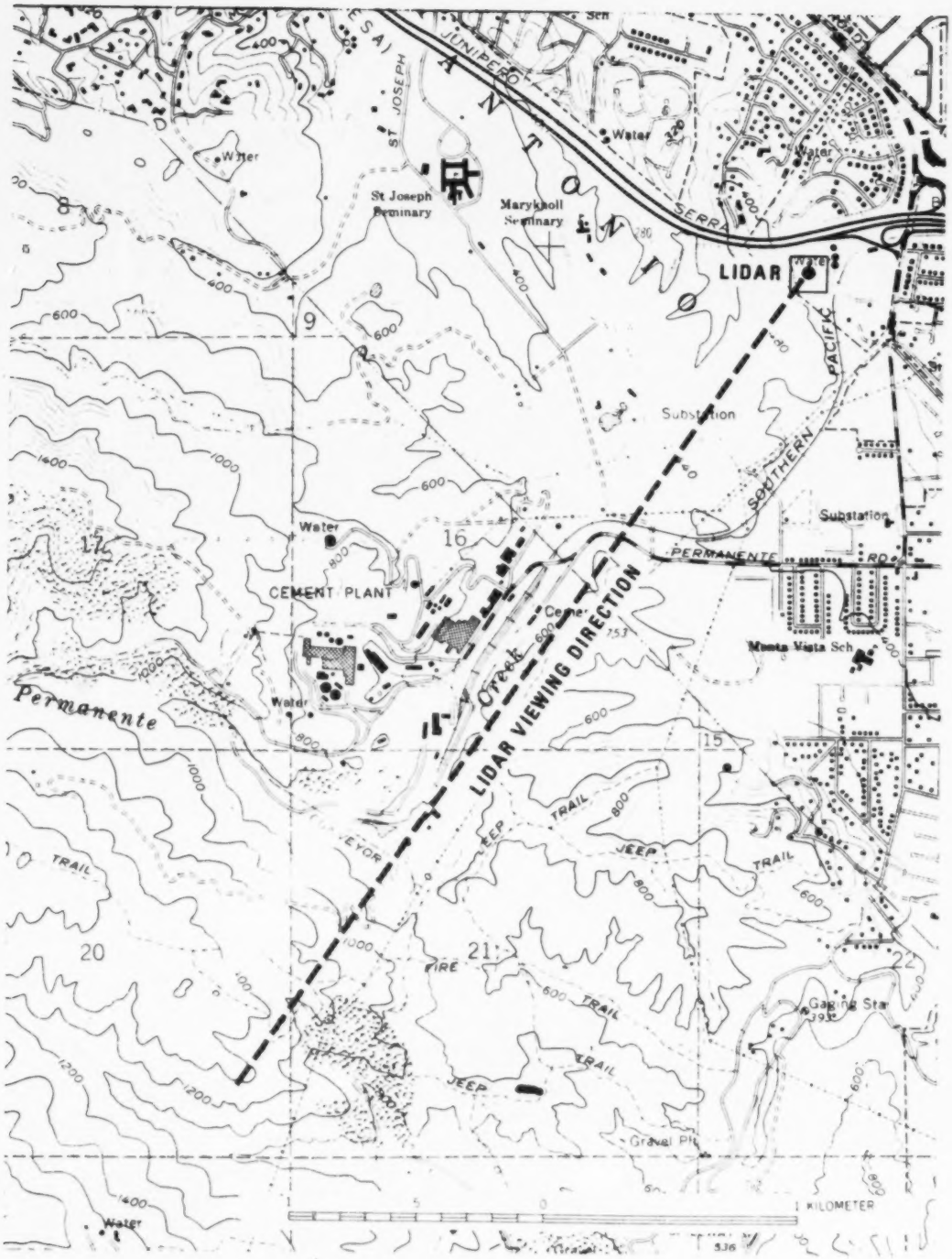

Figure 26. Lidar location and viewing direction during cement plant observations, 21 May 1980.

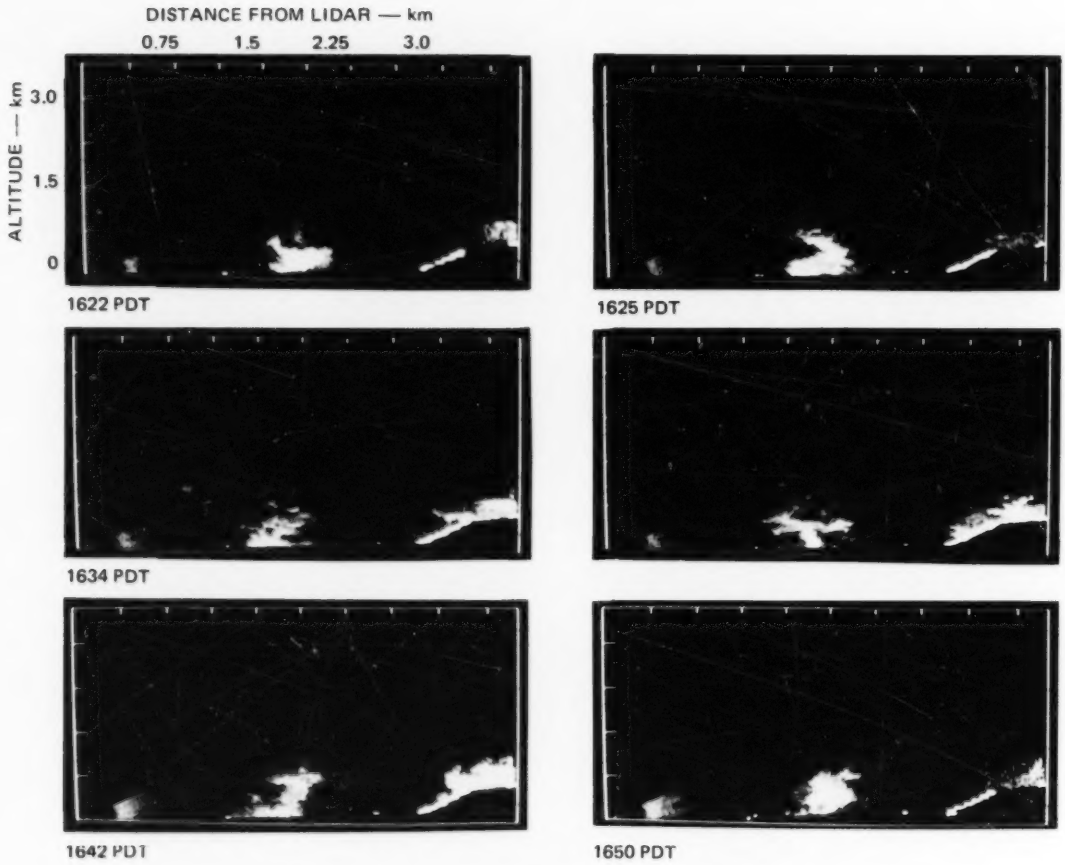

Figure 27. Vertical plume cross sections made about 500 m downwind of the Permanente Cement Plant on 21 May 1980.

Height and distance above lidar are indicated on the first cross section; observation time is given under each cross section.

REFERENCES

Uthe, E.E., N.B. Nielsen, and W.L. Jimison, 1980: "Airborne Lidar Plume and Haze Analyzer (ALPHA-1)," Bull. Am. Met. Soc., Vol. 61, pp. 1035-1043.

Conner, W.D., and N. White, 1980: "Comparative Study of Plume Opacity Measurement Methods," Report EPA-600/2-80-001, Environmental Protection Agency, Environmental Sciences Research Laboratory, Research Triangle Park, North Carolina 27711.

Cook, C.S., G.W. Bethke, and W.D. Conner, 1972: "Remote Measurement of Smoke Plume Transmittance Using Lidar," Appl. Opt., Vol. 11, pp. 1742-1748.

Evans, W.E., 1967: "Development of Lidar Stack Effluent Opacity Measuring System," NTS PB 233-135/AS, Springfield, Virginia, 96 pp.

Uthe, E.E., and W.B. Johnson, 1980: "Application of Lidar Techniques to Estimating Atmospheric Dispersion," Final Report to U.S. Nuclear Regulatory Commission, NUREG/CR-1835, Project 2391, SRI International, Menlo Park, California 94025.

APPENDIX

DATA TABULATION

The following pages present in tabular form data obtained during the series of field experiments at Woodland, California, 9-16 August 1979.

Date	Time (PDT)	Smoke Type*	Release Height (m)	Downwind Viewing Direction (deg)	Lidar/ Smoke Distance (m)	Downwind Distance (m)	Mean Wind		Opacity (%)		Emission Rate (g/min)	Lidar Cross-Plume Integrated Backscatter
							Direction (deg)	Speed (mph)	Smoke Reader	Transmis-someter		
9 Aug 1979	1805-1811	ARB-B	10	5	300	30	136	13.8	50	50	7.48	2.008 E+00
							137	12.1				1.856 E+00
							138	11.7				1.645 E+00
							136	12.6				9.165 E+01
	1814-1821	ARB-B	10	5	300	30	140	10.3	80	70	13.2	4.707 E+00
							142	12.4				2.318 E+00
							142	11.8				4.324 E+00
							147	11.3				3.629 E+00
							147	12.3				1.114 E+00
	1826-1831	ARB-B	10	5	300	30	139	12.1	90	90	26.6	5.138 E+00
							139	11.9				4.237 E+00
							142	10.7				5.484 E+00
	1834-1838	ARB-B	10	5	300	30	153	10.9	40	30	3.47	6.289 E-01
							153	11.0				1.425 E+00
							155	12.5				1.934 E+00
	1838-1842	ARB-B	10	21	280	150	158	12.2	40	30	3.47	1.185 E+00
							159	12.4				7.863 E-01
							158	10.6				1.421 E+00
	1847-1852	ARB-B	10	21	380	150	153	11.4	90	90	28.2	1.013 E+01
							152	10.7				9.715 E+00
							151	9.9				1.042 E+01
	1855-1900	ARB-B	10	21	380	150	153	9.9	50	50	6.91	3.532 E+00
							156	9.4				3.301 E+00
							158	9.0				2.673 E+00
	1903-1910	ARB-B	10	21	350	130	152	9.8	75	70	12.1	4.968 E+00
							151	9.2				4.654 E+00
							148	8.7				5.038 E+00
							146	9.2				4.730 E+00
	1917-1922	ARB-W	10	21	350	130	144	8.9	85	90	4.45	3.833 E-01
							140	8.7				2.591 E-01
							141	9.1				2.153 E-01
10 Aug 1979	1646-1651	1P	5	20	320	120	132	11.1	45		45	4.462 E+01
							136	12.3				6.000 E+01
							131	12.2				3.593 E+01
	1656-1701	2P	5	20	320	120	131	12.5	60-65		90	4.351 E+01
							134	13.2				2.976 E+01
							134	11.2				4.431 E+01

Date	Time (PDT)	Smoke Type*	Release Height (m)	Downwind Viewing Direction (deg)	Lidar/ Smoke Distance (m)	Downwind Distance (m)	Mean Wind		Opacity (%)		Emission Rate (g/min)	Lidar Cross-Plume Integrated Backscatter
							Direction (deg)	Speed (mph)	Smoke Reader	Transmis-someter		
10 Aug 1979	1711-1718	4P	5	20	320	120	135	15.2	60-70		180	4.802 E+01
							140	14.6				7.893 E+01
							139	14.0				9.333 E+01
							138	13.0				6.829 E+01
	1724-1731	8P	5	20	320	120	157	13.9	90		360	1.195 E+02
							148	13.6				7.482 E+01
							157	13.0				1.389 E+02
							149	12.3				7.711 E+01
	1738-1745	1P	5	30	380	220	155	13.5	20-25		45	2.907 E+01
							147	10.8				4.079 E+01
							140	12.0				3.274 E+01
							141	13.1				5.283 E+01
	1748-1754	2P	5	30	380	220	141	12.4	70		90	9.712 E+01
							136	13.4				1.103 E+02
							136	12.6				8.620 E+01
	1759-1806	4P	5	30	370	210	138	12.8	75-80		180	1.059 E+02
							138	14.6				1.224 E+02
							139	13.6				1.143 E+02
							138	13.3				1.163 E+02
	1812-1818	8P	5	30	370	210	137	12.5	90		360	1.473 E+02
							135	12.7				1.514 E+02
							135	12.6				1.542 E+02
	1827-1833	1P	1	30	350	200	150	12.1	40		45	5.738 E+01
							151	11.4				7.464 E+01
							149	12.2				6.400 E+01
	1836-1840	2P	1	30	350	200	143	9.5	90		90	1.152 E+02
							137	10.1				1.005 E+02
	1845-1852	4P	1	30	350	200	136	11.8	80		180	1.187 E+02
							136	10.8				8.201 E+01
							135	11.3				9.399 E+01
							137	11.9				9.153 E+01
	1856-1902	8P	1	30	350	200	139	11.2	90		360	1.112 E+02
							139	10.2				1.169 E+02
							138	10.0				1.302 E+02

Date	Time (PDT)	Smoke Type*	Release Height (m)	Downwind Viewing Direction (deg)	Lidar Smoke Distance (m)	Downwind Distance (m)	Mean Wind		Opacity (%)		Emission Rate (g/min)	Lidar Cross-Plume Integrated Backscatter
							Direction (deg)	Speed (mph)	Smoke Reader	Transmis-someter		
16 Aug 1979	1702-1713†	1P	5	30	320	180	135	17.2	30		45	1.201 E+02
							126	14.2				1.385 E+02
							128	14.6				1.668 E+02
	1717-1723†	2P	5	30	330	180	128	15.4	50		90	2.663 E+02
							129	15.2				2.503 E+02
							132	15.7				1.799 E+02
	1740-1745†	4P	5	30	330	180	147	17.3	70		180	2.645 E+02
							150	16.8				3.127 E+02
							155	15.4				5.407 E+02
	1752-1756†	8P	5	30	340	200	138	13.2	90		360	4.094 E+02
							144	15.3				7.960 E+02
							139	15.8				5.831 E+02
	1838-1845	1P	5	30	330	180	152	12.3	25		45	8.788 E+01
							155	11.1				5.691 E+01
							152	10.9				5.997 E+01
							151	11.1				9.667 E+01
							151	14.7				1.937 E+01
	1908-1913	2P	5	30	370	210	158	16.3	55		90	3.105 E+02
							160	18.4				1.738 E+02
							160	17.0				1.922 E+02
15 Aug 1979	1923-1927	1C	5	30	400	230	154	9.6	10		10	7.240 E+00
							153	10.5				2.093 E+01
							155	11.3				2.194 E+01
	1928-1932	2C	5	30	350	200	151	12.1	20		20	3.092 E+01
							140	10.0				4.506 E+01
							143	9.6				7.609 E+01
	1938-1942	4C	5	30	350	200	148	9.5	35		40	5.909 E+01
							147	10.1				7.515 E+01
							149	12.4				7.015 E+01
	1946-1949	8C	5	30	350	200	149	12.4	50		80	1.056 E+02
							140	11.4				1.737 E+02
							139	10.2				1.936 E+02
16 Aug 1979	1832-1836	1C	5	30	320	180	152	13.3	10		10	4.939 E+01
							154	14.3				3.104 E+01

Date	Time (PDT)	Smoke Type*	Release Height (m)	Downwind Viewing Direction (deg)	Lidar/ Smoke Distance (m)	Downwind Distance (m)	Mean Wind		Opacity (%)		Emission Rate (g/min)	Lidar Cross-Plume Integrated Backscatter
							Direction (deg)	Speed (mph)	Smoke Reader	Transmis-someter		
16 Aug 1979	1845-1853	2C	5	30	350	200	159	10.5	20		20	3.913 E+01
							159	13.5				4.725 E+01
							153	12.6				6.578 E+01
	1935-1940	1C	1	30	450	260	158	12.8	20		10	1.584 E+01
							167	13.8				4.572 E+01
							163	12.9				3.034 E+01
	1942-1948	2C	1	30	400	230	163	13.6	35		20	4.983 E+01
							164	13.3				3.751 E+01
							163	15.9				3.508 E+01
							163	14.1				4.016 E+01
	1950-1954	4C	1	30	450	260	161	14.3	75		40	1.036 E+02‡
							160	12.8				4.458 E+01‡
							164	13.7				8.501 E+01‡
							163	11.9				7.673 E+01‡
	1958-2008	8C	1	30	450	260	159	10.7	85		80	1.297 E+02
							160	10.6				1.505 E+02
							158	11.0				1.260 E+02
							160	11.5				1.115 E+02

*ARB-W = CARB generator white smoke, ARB-B = CARB generator black smoke, P = smoke pots, and C = smoke candles.

'New log amp 1702-1756 only.

‡Road dust included in integration.